of age, plasma sSMase activity was lower in apoE$^{-/-}$ than that in WT.

Aortic aSMase activity in WT was significantly elevated at 15 w of age compared with the level observed at 7 w of age, the level increased further at 65 w of age (Table 1). In contrast, aortic aSMase activity in apoE$^{-/-}$ was unchanged at 15 w of age compared with that at 7 w of age and declined significantly at 65 w of age. Liver aSMase and neutral SMase activities were unchanged during aging in both apoE$^{-/-}$ and WT (data not shown).

Changes in Tissue Ceramide Levels The total aortic ceramide level in WT at 65 w of age increased significantly compared with that observed at 7 w of age (2.6-fold increase) (Table 2A). In the apoE$^{-/-}$ aorta, the total ceramide level was increased at 15 w and 65 w of age compared with the level observed at 7 w of age (2.0, 1.9-fold, respectively). The total aortic ceramide concentration of apoE$^{-/-}$ was similar to that of WT at 7 w of age (Table 2A); however, it was significantly higher than that of WT (2.7-fold) at 15 w of age. Table 2A demonstrates the six major ceramide levels. In the WT aorta, C24:0, C24:1, and C24:2 ceramide levels at 65 w of age were significantly higher than those at 7 w of age (2.6, 2.9, 6.0-fold, respectively). In contrast, C18:0, C22:0, and C24:0 ceramide levels in apoE$^{-/-}$ aorta increased at 15 w of age compared with those observed at 7 w of age (2.7, 2.4, 2.2-fold, respectively). The C16:0, C24:1, and C24:2 ceramide levels in apoE$^{-/-}$ aorta at 65 w of age increased compared with those at 7 w of age (2.5, 2.3, 2.6-fold, respectively) (Table 2A).

Although the levels of almost all ceramide species changed in a similar manner to the total level, some ceramides showed a different behavior (Table 2A). The levels of C16:0, C18:0, C22:0, and C24:0 ceramides in the apoE$^{-/-}$ aorta were significantly higher than those of WT (2.4, 4.1, 3.5, 3.5-fold, respectively) at 15 w of age.

The total plasma ceramide level in apoE$^{-/-}$ was significantly higher (4.4–5.9-fold) than that observed in WT at all ages

Table 2A. Levels of Ceramides in the Aorta of Wild-Type and ApoE$^{-/-}$ Mice

(A) Aorta ceramide levels (nmol/mg protein)

Aorta	7w WT	15w WT	65w WT	7w apoE$^{-/-}$	15w apoE$^{-/-}$	65w apoE$^{-/-}$
C16:0	1.08±0.18^{a}	1.53±0.15^{a}	2.48±0.32^{ac}	2.03±0.46^{ac}	3.70±0.52^{bc}	4.98±0.53^{b}
C18:0	0.38±0.04^{a}	0.38±0.03^{a}	0.74±0.07^{a}	0.58±0.14^{a}	1.53±0.14^{b}	0.47±0.04^{a}
C22:0	0.45±0.06^{ab}	0.44±0.05^{b}	0.95±0.13^{a}	0.66±0.14^{ab}	1.56±0.18^{bc}	0.94±0.08^{a}
C24:0	1.36±0.21^{ac}	1.33±0.10^{a}	3.52±0.46^{bd}	2.10±0.39^{ad}	4.69±0.55^{b}	3.03±0.29^{cd}
C24:1	0.58±0.12^{a}	1.03±0.12^{ab}	1.70±0.15^{b}	1.22±0.24^{ab}	1.79±0.25^{b}	2.82±0.31^{c}
C24:2	0.17±0.03^{a}	0.39±0.06^{a}	1.02±0.13^{b}	0.45±0.08^{a}	0.50±0.10^{a}	1.15±0.13^{b}
Total	4.02±0.58^{a}	5.09±0.48^{a}	10.40±1.17^{bc}	7.03±1.42^{ab}	13.77±1.73^{cd}	13.39±1.23^{cd}

Values are presented as mean±S.E.M. for 4 or 5 animals in each group. Total values are sum of six ceramide species. Different superscript letters indicate significant differences at $p<0.05$ (Tukey–Kramer *post hoc* test).

Table 2B. Levels of Ceramides in the Plasma of Wild-Type and ApoE$^{-/-}$ Mice

(B) Plasma ceramide levels (nmol/mL)

Plasma	7w WT	15w WT	65w WT	7w apoE$^{-/-}$	15w apoE$^{-/-}$	65w apoE$^{-/-}$
C16:0	0.53±0.04^{a}	0.50±0.09^{a}	0.47±0.05^{a}	5.63±0.42^{b}	4.33±0.26^{c}	3.34±0.39^{c}
C18:0	0.14±0.03^{a}	0.20±0.03^{a}	0.16±0.02^{a}	0.82±0.10^{b}	0.85±0.05^{b}	0.47±0.07^{c}
C22:0	1.06±0.12^{a}	0.98±0.15^{a}	0.79±0.06^{a}	8.50±1.12^{b}	6.61±0.44^{b}	3.77±0.26^{c}
C24:0	4.86±0.48^{a}	3.89±0.68^{a}	2.96±0.38^{a}	25.76±3.44^{b}	16.81±0.82^{c}	12.08±0.64^{c}
C24:1	2.82±0.46^{a}	3.20±0.55^{a}	2.33±0.24^{a}	14.84±1.90^{b}	12.93±0.58^{bc}	9.43±0.59^{c}
C24:2	0.20±0.05^{a}	0.22±0.04^{a}	0.21±0.02^{a}	1.05±0.05^{a}	1.01±0.07^{ab}	1.37±0.44^{b}
Total	9.62±1.14^{a}	8.99±1.48^{a}	6.92±0.72^{a}	56.60±6.54^{b}	42.53±1.81^{c}	30.46±1.74^{c}

Values are presented as mean±S.E.M. for 4 or 5 animals in each group. Total values are sum of six ceramide species. Different superscript letters indicate significant differences at $p<0.05$ (Tukey–Kramer *post hoc* test).

Table 2C. Levels of Ceramides in the Liver of Wild-Type and ApoE$^{-/-}$ Mice

(C) Liver ceramide levels (nmol/g tissue)

Liver	7w WT	15w WT	65w WT	7w apoE$^{-/-}$	15w apoE$^{-/-}$	65w apoE$^{-/-}$
C16:0	47.03±4.12^{a}	72.29±5.66^{b}	60.20±5.22^{ab}	52.47±4.87^{ab}	56.07±2.02^{ab}	55.09±3.71^{ab}
C18:0	8.03±0.85^{a}	16.48±2.15^{b}	13.10±0.29^{ab}	10.19±1.54^{a}	12.02±1.35^{ab}	8.07±0.98^{a}
C22:0	44.14±1.96^{a}	65.93±3.69^{b}	67.06±3.28^{b}	66.16±7.25^{b}	65.48±4.23^{b}	38.75±2.36^{a}
C24:0	128.87±5.43^{ab}	169.37±10.78^{a}	156.39±16.47^{ab}	178.40±19.69^{a}	153.40±6.30^{ab}	105.94±4.78^{b}
C24:1	201.38±11.52^{a}	283.16±13.98^{b}	239.44±12.91^{ab}	200.30±8.90^{a}	247.01±11.85^{ab}	208.74±10.94^{a}
C24:2	16.67±0.97	22.33±1.70	20.40±3.24	21.30±1.83	24.23±1.11	24.11±3.87
Total	446.12±22.95^{ac}	629.55±29.14^{b}	556.58±26.09^{ab}	528.82±35.68^{abc}	558.22±15.30^{ab}	440.69±19.06^{c}

Values are presented as mean±S.E.M. for 4 or 5 animals in each group. Total values are sum of six ceramide species. Different superscript letters indicate significant differences at $p<0.05$ (Tukey–Kramer *post hoc* test).

(Table 2B). Almost all plasma ceramide species in apoE$^{-/-}$ decreased with age with the exception of C24:2 ceramide (Table 2B).

The total ceramide level in WT liver increased at 15 w at age (Table 2C) and the levels of C16:0, C18:0, C22:0, and C24:1 ceramides were highest at 15 w of age (Table 2C). In apoE$^{-/-}$ liver, C22:0 ceramide level at 7 w of age was significantly higher than that observed in WT, whereas C22:0 ceramide level and total ceramide level at 65 w of age were significantly lower in apoE$^{-/-}$ than those in WT.

DISCUSSION

The total plasma ceramide level in apoE$^{-/-}$ was comparable to that reported for human atherosclerotic subjects,[14] and was significantly higher than the level observed in WT at all ages, indicating that the aorta of apoE$^{-/-}$ was exposed to a higher plasma ceramide level throughout aging. The difference in the plasma ceramide levels between WT and apoE$^{-/-}$ may be attributed to the LDL level in plasma because LDL is the major ceramide carrier.[27,28] The plasma ceramide level correlated with the LDL cholesterol and oxLDL levels in human samples.[14] The plasma ceramide level in apoE$^{-/-}$ decreased during aging. As a similar phenomemon was reported for oxLDL by Itabe and colleagues[29]: the level of oxLDL increased at 20 w of age and decreased toward the basal level at 40 w of age in apoE$^{-/-}$. These authors suggested that oxLDL appeared before the development of atherosclerotic lesions. Moreover, Schissel *et al.*[30] indicated that ceramides, generated by sSMase from the lesional LDL, but not from the plasma LDL, participated in LDL aggregation. Combining these reports with the results from this study, in which aortic ceramide levels increased at 15 w of age in apoE$^{-/-}$, it is suggested that an elevation in ceramide level at the beginning of atherogenesis is involved in the pathogenesis of atherosclerosis.

Although the aortic ceramide level increased significantly in both WT and apoE$^{-/-}$, the distribution pattern of ceramide species in WT and apoE$^{-/-}$ was different. At 15 w of age, when atherogenesis was assumed to initiate in apoE$^{-/-}$,[31,32] the levels of C16:0, C18:0, C22:0, and C24:0 ceramides in the aorta increased significantly, whereas only C16:0 and C24:1 ceramide levels increased at 65 w of age. The aortic levels of C18:0, C22:0, and C24:0 ceramides caused a similar change in aortic SMase activity. On the basis of these results, we suggest that the increase in C18-24 ceramide levels and the elevation of aortic aSMase activity may play a role in the initiation of atherogenesis. In addition, this is the first study showing elevation of aortic ceramide level during aging in apoE$^{-/-}$ as well as in WT.

In contrast to C24 ceramide, C16:0 ceramide, a major ceramide in the aorta of apoE$^{-/-}$ that increased at 15 and 65 w of age, seemed to have a different function. Ceramide chain length affects the physicochemical properties of lipid membranes;[33] thus, C16:0 ceramide easily mixes with cholesterol in contrast to C24 ceramide.[34] Mesicek *et al.*[35] reported that the overexpression of ceramide synthase (CerS) 5 lead to generation of C16:0 ceramide and an increase in apoptosis, whereas overexpression of CerS2 yielded C24 ceramide and provoked pro-survival signals. Furthermore, in the liver of CerS2 null mice, elevated ROS levels are associated with an increase in C16:0 ceramide and a decrease in mitochondria complex IV activity.[36] In this regard, cellular homeostasis appears to be maintained by a balance between C16:0 and C24:0 ceramides. Although the present study showed that C16:0 ceramide behaved in a manner similar to the very long, unsaturated C24:1 ceramide, the relationship between atherogenesis and apoptosis caused by ceramides, particularly C16:0 and C24 ceramides, requires further examination.

Liver ceramide levels were unchanged with aging in either apoE$^{-/-}$ or WT. Similar results were obtained in diabetic rats.[17] These observations suggested that aging did not affect hepatic ceramide metabolism.

In conclusion, this study suggests that elevation of ceramide species such as C16:0 in the aorta as a result of sSMase activity in the plasma contributes to atherogenesis during aging.

Acknowledgment This work was supported by Grant-in-Aid from the Ministry of Education, Culture, Sports, Science and Technology of Japan.

REFERENCES

1) Hannun YA, Obeid LM. The ceramide-centric universe of lipid-mediated cell regulation: stress encounters of the lipid kind. *J. Biol. Chem.*, **277**, 25847–25850 (2002).
2) Kolesnick R. Ceramide: a novel second messenger. *Trends Cell Biol.*, **2**, 232–236 (1992).
3) Farrell AM, Uchida Y, Nagiec MM, Harris IR, Dickson RC, Elias PM, Holleran WM. UVB irradiation up-regulates serine palmitoyltransferase in cultured human keratinocytes. *J. Lipid Res.*, **39**, 2031–2038 (1998).
4) Santana P, Peña LA, Haimovitz-Friedman A, Martin S, Green D, McLoughlin M, Cordon-Cardo C, Schuchman EH, Fuks Z, Kolesnick R. Acid sphingomyelinase-deficient human lymphoblasts and mice are defective in radiation-induced apoptosis. *Cell*, **86**, 189–199 (1996).
5) Merrill AH Jr, Jones DD. An update of the enzymology and regulation of sphingomyelin metabolism. *Biochim. Biophys. Acta*, **1044**, 1–12 (1990).
6) Yamada Y, Kajiwara K, Yano M, Kishida E, Masuzawa Y, Kojo S. Increase of ceramides and its inhibition by catalase during chemically induced apoptosis of HL-60 cells determined by electrospray ionization tandem mass spectrometry. *Biochim. Biophys. Acta*, **1532**, 115–120 (2001).
7) Goñi FM, Alonso A. Sphingomyelinases: enzymology and membrane activity. *FEBS Lett.*, **531**, 38–46 (2002).
8) Schuchman EH. Acid sphingomyelinase, cell membranes and human disease: lessons from Niemann–Pick disease. *FEBS Lett.*, **584**, 1895–1900 (2010).
9) Schissel SL, Keesler GA, Schuchman EH, Williams KJ, Tabas I. The cellular trafficking and zinc dependence of secretory and lysosomal sphingomyelinase, two products of the acid sphingomyelinase gene. *J. Biol. Chem.*, **273**, 18250–18259 (1998).
10) Jenkins RW, Canals D, Idkowiak-Baldys J, Simbari F, Roddy P, Perry DM, Kitatani K, Luberto C, Hannun YA. Regulated secretion of acid sphingomyelinase: implications for selectivity of ceramide formation. *J. Biol. Chem.*, **285**, 35706–35718 (2010).
11) Tabas I. Secretory sphingomyelinase. *Chem. Phys. Lipids*, **102**, 123–130 (1999).
12) Walters MJ, Wrenn SP. Effect of sphingomyelinase-mediated generation of ceramide on aggregation of low-density lipoprotein. *Langmuir*, **24**, 9642–9647 (2008).
13) Morita SY, Kawabe M, Sakurai A, Okuhira K, Vertut-Doï A, Nakano M, Handa T. Ceramide in lipid particles enhances heparan sulfate proteoglycan and low density lipoprotein receptor-related

protein-mediated uptake by macrophages. *J. Biol. Chem.*, **279**, 24355–24361 (2004).
14) Ichi I, Nakahara K, Miyashita Y, Hidaka A, Kutsukake S, Inoue K, Maruyama T, Miwa Y, Harada-Shiba M, Tsushima M, Kojo S, Kisei Cohort Study Grooup. Association of ceramides in human plasma with risk factors of atherosclerosis. *Lipids*, **41**, 859–863 (2006).
15) Deevska GM, Sunkara M, Morris AJ, Nikolova-Karakashian MN. Characterization of secretory sphingomyelinase activity, lipoprotein sphingolipid content and LDL aggregation in $ldlr^{-/-}$ mice fed on a high-fat diet. *Biosci. Rep.*, **32**, 479–490 (2012).
16) Ichi I, Takashima Y, Adachi N, Nakahara K, Kamikawa C, Harada-Shiba M, Kojo S. Effects of dietary cholesterol on tissue ceramides and oxidation products of apolipoprotein B-100 in ApoE-deficient mice. *Lipids*, **42**, 893–900 (2007).
17) Kobayashi K, Ichi I, Nakagawa T, Kamikawa C, Kitamura Y, Koga E, Washino Y, Hoshinaga Y, Kojo S. Increase in plasma ceramide levels *via* secretory sphingomyelinase activity in streptozotocin-induced diabetic rats. *Med. Chem. Commun.*, **2**, 536–541 (2011).
18) Doehner W, Bunck AC, Rauchhaus M, von Haehling S, Brunkhorst FM, Cicoira M, Tschope C, Ponikowski P, Claus RA, Anker SD. Secretory sphingomyelinase is upregulated in chronic heart failure: a second messenger system of immune activation relates to body composition, muscular functional capacity, and peripheral blood flow. *Eur. Heart J.*, **28**, 821–828 (2007).
19) Górska M, Barańczuk E, Dobrzyń A. Secretory Zn^{2+}-dependent sphingomyelinase activity in the serum of patients with type 2 diabetes is elevated. *Horm. Metab. Res.*, **35**, 506–507 (2003).
20) Filosto S, Fry W, Knowlton AA, Goldkorn T. Neutral sphingomyelinase 2 (nSMase2) is a phosphoprotein regulated by calcineurin (PP2B). *J. Biol. Chem.*, **285**, 10213–10222 (2010).
21) Ichi I, Kamikawa C, Nakagawa T, Kobayashi K, Kataoka R, Nagata E, Kitamura Y, Nakazaki C, Matsura T, Kojo S. Neutral sphingomyelinase-induced ceramide accumulation by oxidative stress during carbon tetrachloride intoxication. *Toxicology*, **261**, 33–40 (2009).
22) Lightle SA, Oakley JI, Nikolova-Karakashian MN. Activation of sphingolipid turnover and chronic generation of ceramide and sphingosine in liver during aging. *Mech. Ageing Dev.*, **120**, 111–125 (2000).
23) Lowry OH, Rosebrough NJ, Farr AL, Randall RJ. Protein measurement with the Folin phenol reagent. *J. Biol. Chem.*, **193**, 265–275 (1951).
24) Bligh EG, Dyer WJ. A rapid method of total lipid extraction and purification. *Can. J. Biochem. Physiol.*, **37**, 911–917 (1959).
25) Folch J, Ascoli I, Lees M, Meath JA, LeBaron N. Preparation of lipid extracts from brain tissue. *J. Biol. Chem.*, **191**, 833–841 (1951).
26) Yano M, Kishida E, Muneyuki Y, Masuzawa Y. Quantitative analysis of ceramide molecular species by high performance liquid chromatography. *J. Lipid Res.*, **39**, 2091–2098 (1998).
27) Wiesner P, Leidl K, Boettcher A, Schmitz G, Liebisch G. Lipid profiling of FPLC-separated lipoprotein fractions by electrospray ionization tandem mass spectrometry. *J. Lipid Res.*, **50**, 574–585 (2009).
28) Hammad SM, Pierce JS, Soodavar F, Smith KJ, Al Gadban MM, Rembiesa B, Klein RL, Hannun YA, Bielawski J, Bielawska A. Blood sphingolipidomics in healthy humans: impact of sample collection methodology. *J. Lipid Res.*, **51**, 3074–3087 (2010).
29) Kato R, Mori C, Kitazato K, Arata S, Obama T, Mori M, Takahashi K, Aiuchi T, Takano T, Itabe H. Transient increase in plasma oxidized LDL during the progression of atherosclerosis in apolipoprotein E knockout mice. *Arterioscler. Thromb. Vasc. Biol.*, **29**, 33–39 (2009).
30) Schissel SL, Tweedie-Hardman J, Rapp JH, Graham G, Williams KJ, Tabas I. Rabbit aorta and human atherosclerotic lesions hydrolyze the sphingomyelin of retained low-density lipoprotein. Proposed role for arterial-wall sphingomyelinase in subendothelial retention and aggregation of atherogenic lipoproteins. *J. Clin. Invest.*, **98**, 1455–1464 (1996).
31) Plump AS, Smith JD, Hayek T, Aalto-Setälä K, Walsh A, Verstuyft JG, Rubin EM, Breslow JL. Severe hypercholesterolemia and atherosclerosis in apolipoprotein E-deficient mice created by homologous recombination in ES cells. *Cell*, **71**, 343–353 (1992).
32) Zhang SH, Reddick RL, Piedrahita JA, Maeda N. Spontaneous hypercholesterolemia and arterial lesions in mice lacking apolipoprotein E. *Science*, **258**, 468–471 (1992).
33) Grösch S, Schiffmann S, Geisslinger G. Chain length-specific properties of ceramides. *Prog. Lipid Res.*, **51**, 50–62 (2012).
34) ten Grotenhuis E, Demel RA, Ponec M, Boer DR, van Miltenburg JC, Bouwstra JA. Phase behavior of stratum corneum lipids in mixed Langmuir–Blodgett monolayers. *Biophys. J.*, **71**, 1389–1399 (1996).
35) Mesicek J, Lee H, Feldman T, Jiang X, Skobeleva A, Berdyshev EV, Haimovitz-Fridman A, Fuks Z, Kolesnick R. Ceramide synthases 2, 5, and 6 confer distinct roles in radiation-induced apoptosis in HeLa cells. *Cell. Signal.*, **22**, 1300–1307 (2010).
36) Zigdon H, Kogot-Levin A, Park JW, Goldschmidt R, Kelly S, Merrill AH Jr, Scherz A, Pewzner-Jung Y, Saada A, Futerman AH. Ablation of ceramide synthase 2 causes chronic oxidative stress due to disruption of the mitochondrial respiratory chain. *J. Biol. Chem.*, **288**, 4947–4956 (2013).

INTERNAL MEDICINE

□ CASE REPORT □

Familial Hypercholesterolemia with Multiple Large Tendinous Xanthomas and Advanced Coronary Artery Atherosclerosis

Fumio Terasaki[1], Hideaki Morita[1], Mariko Harada-Shiba[2], Naotaka Ohta[3], Kaoru Otsuka[1], Shinpei Nogi[1], Masatoshi Miyamura[1], Shuji Suzuki[1], Takahide Ito[1], Hiroaki Shimomura[4], Takahiro Katsumata[5], Yoshihiro Miyamoto[2] and Nobukazu Ishizaka[1]

Abstract

We herein report the case of a 53-year-old man with severe coronary ischemia who underwent successful coronary artery bypass surgery. Of note, he had hypercholesterolemia and presented with multiple large tendinous xanthomas and thickened Achilles tendons that had been present for more than two decades. Together with a family history of dyslipidemia, the patient was diagnosed as having familial hypercholesterolemia. Irrespective of an extensive search for possible mutations in the genes presumably involved in the patient's pathophysiology, including low-density lipoprotein receptor (LDLR), proprotein convertase subtilisin/kexin type 9 (PCSK9), autosomal recessive hypercholesterolemia (ARH) and apolipoprotein B (APOB), we were not able to identify the gene mutations responsible for the phenotype observed in the present case.

Key words: familial hypercholesterolemia, tendinous xanthomas, coronary artery disease

(Intern Med 52: 577-581, 2013)
(DOI: 10.2169/internalmedicine.52.8522)

Introduction

Familial hypercholesterolemia (FH) is characterized by increased levels of serum low-density lipoprotein (LDL) cholesterol with a high prevalence of coronary atherosclerosis. It may be inherited as an autosomal dominant trait, and the frequencies of homo- and heterozygotes are estimated to be $1/1\times10^6$ and 1/500, respectively, in the general population. Establishing a diagnosis in these patients is important because lipid-lowering therapy not only slows the progression of atherosclerosis, but also may achieve regression of atherosclerotic vascular lesions. Genetically determining the presence of FH is feasible, although testing is not yet available for routine use. In a large portion of patients, the diagnosis of heterozygous FH is based on laboratory and clinical criteria (1, 2).

Case Report

A 33-year-old man was diagnosed as having hypercholesterolemia more than two decades ago. The lipid profile of his mother at 72 years of age was as follows: total cholesterol, 257 mg/dL; LDL cholesterol, 167 mg/dL; high density lipoprotein (HDL) cholesterol, 72 mg/dL; and triglycerides 138 mg/dL. She was not taking any lipid-lowering drugs nor did she have xanthomas. We could not obtain information regarding abnormal lipid metabolism from other family members. Since then, multiple subcutaneous nodular tumorous lesions began to develop in the present patient and grew larger on the sites of the bilateral Achilles tendons, the ulnar side of the right wrist, the dorsum of the right hand and the

[1]Department of Cardiology, Osaka Medical College, Japan, [2]Department of Molecular Innovation in Lipidology, National Cerebral and Cardiovascular Center Research Institute, Japan, [3]Laboratory of Molecular Genetics, National Cerebral and Cardiovascular Center Research Institute, Japan, [4]Department of Internal Medicine, Arisawa General Hospital, Japan and [5]Department of Cardiovascular Surgery, Osaka Medical College, Japan

Received for publication July 4, 2012; Accepted for publication November 27, 2012

Correspondence to Dr. Fumio Terasaki, in3012@poh.osaka-med.ac.jp

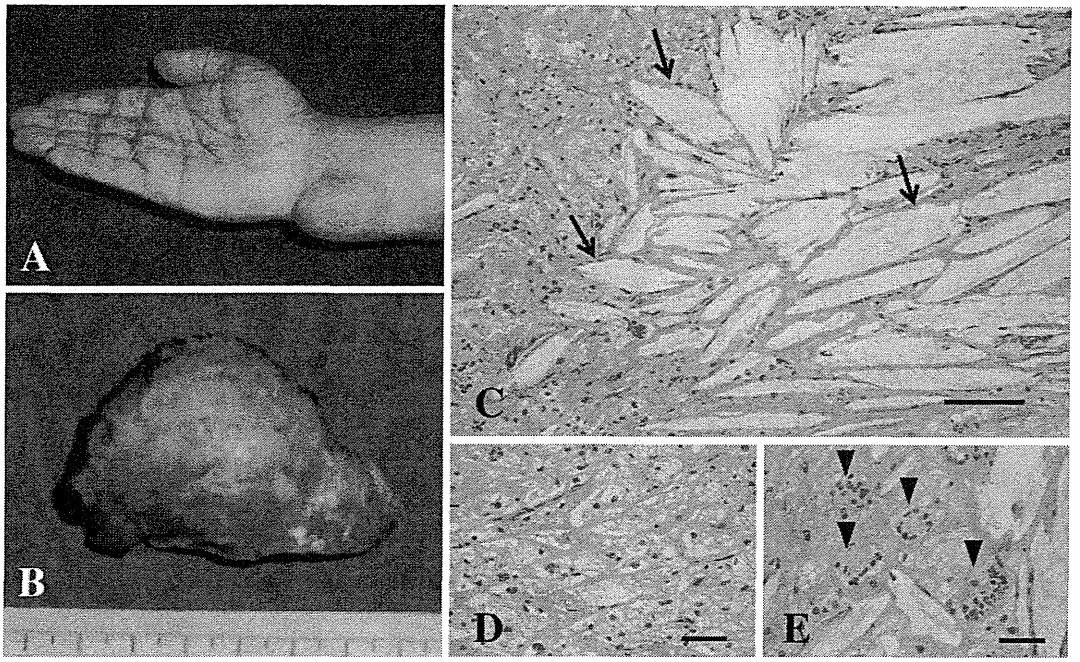

Figure 1. A nodular tumor on the ulnar side of the right wrist observed in 1999 (A). The resected tumor measured 6.0 cm × 3.5 cm in size and was yellowish and lustrous (B). A microscopic examination of the resected tumor revealed numerous extracellular cholesterol deposits (cholesterol clefts) (arrows in C) and diffuse sheets of foamy cells (xanthoma cells) (D) within fibrous tissue. Multinucleated giant cells were also conspicuous (arrowheads in E). The scale bar indicates 100 μm in C (magnification: ×40) and 50 μm in D, E (magnification: ×100).

left fingers. These subcutaneous tumors grew up to the size of a ping-pong ball or an egg. In 1999, at 41 years of age, the patient was admitted to the orthopedics department where some of the subcutaneous tumorous lesions were surgically resected (Fig. 1A, B). A histological examination of the resected specimens revealed numerous extracellular cholesterol (cholesterol clefts) and diffuse sheets of foamy cells (xanthoma cells) interspersed with inflammatory cells within fibrous tissue. Multinucleated giant cells were also conspicuous (Fig. 1C-E). A diagnosis of tendinous xanthomas was then made. The patient's serum LDL cholesterol level was 193 mg/dL at that time, and statin therapy was started thereafter. Meanwhile, however, he did not continue to visit the hospital regularly; therefore, the statin therapy was discontinued 12 years prior to the patient's admission to our hospital in 2010.

In 2007, at 50 years of age, the patient was again diagnosed as having hypercholesterolemia and diabetes mellitus at a routine health check-up; however, medical treatment was not started at that time. In October 2009, he began to experience chest oppression on exertion. The chest pain was associated with cold sweating and subsided when the patient was at rest for five minutes. In May 2010, the duration of chest pain became prolonged up to 20 to 30 minutes and the frequency increased up to three to four times per day. The patient visited a regional hospital where electrocardiogram showed ST-T segment changes suggestive of the presence of unstable angina pectoris. He was immediately hospitalized and an intravenous infusion of heparin sodium and isosorbide dinitrate was started, which markedly, but not completely, relieved his symptoms. He was then transferred to our hospital for further evaluation and treatment.

On admission, the patient's consciousness was clear, his body temperature was 36.8 degrees and his blood pressure was 108/72 mmHg. His heart sounds were normal and no abnormal heart murmurs were audible. No abnormal neurological findings were noted. Chest X-ray and electrocardiogram showed no significant abnormalities on admission. Multiple nodular subcutaneous tumors were observed on the dorsum of the bilateral hands, the bilateral wrists, the soles of the bilateral feet and the bilateral Achilles tendons (Fig. 2A, B). Severe thickening of the bilateral Achilles tendons (right side: 40 mm, left side: 30 mm) was confirmed on an X-ray examination (Fig. 2C, D). Echocardiography demonstrated that the aortic valve had three cusps, while valvular calcification was not significant.

The laboratory data obtained on admission are shown in the Table. At the time of admission, the patient began taking lipid- and glucose-lowering drugs, including rosuvastatin calcium (5.0 mg/d), metformin hydrochloride (750 mg/d), pioglitazone hydrochloride (15 mg/d) and glimepiride (3.0 mg/d). He is a former smoker with a Brinkman index of 390. The serum levels of sitosterol and campesterol measured by means of gas chromatography (SRL, Co., Ltd., Tokyo, Japan) were 1.2 μg/mL and 1.9 μg/mL, respectively, neither of which were elevated.

Coronary angiography showed multivessel coronary artery stenosis with 99% stenosis in the right coronary artery

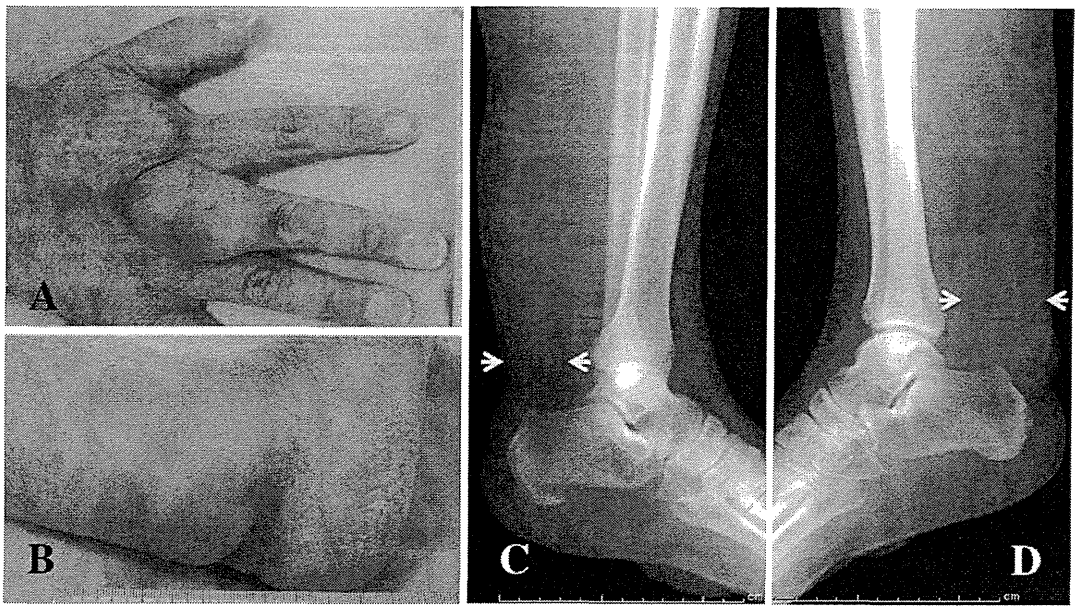

Figure 2. Large nodular tumors on the back side of the right hand (A) and the right Achilles tendon (B) are presented. Radiography of the Achilles tendons showed severe thickening of the bilateral Achilles tendons [left side (arrows in C): 30 mm, right side (arrows in D): 40 mm].

Table. Results of Laboratory Tests on Admission and 1 Month after the Treatment with a Statin and Anti-hyperglycemic Agents

	before	after	normal range
Total Cholesterol	282 mg/dL	137 mg/dL	(130-219)
LDL- Cholesterol	208 mg/dL	71 mg/dL	(70-139)
HDL- Cholesterol	45 mg/dL	41 mg/dL	(40-77)
Triglyceride	143 mg/dL	124 mg/dL	(30-149)
Apolipoprotein B	NE	79 mg/dL	(73-109)
Lipoprotein (a)	NE	23 mg/dL	(< 30)
Glucose	232 mg/dL	96 mg/dL	(60-109)
HbA1c (JDS)	9.3 %	6.2 %	(4.3-5.8)

NE: not examined, JDS: Japan Diabetes Society

(RCA), 90% stenosis in the left anterior descending artery (LAD) and 99% stenosis in the left circumflex artery (LCX) (Fig. 3A, B). No significant luminal stenosis was seen near the ostial lesions of the right or left coronary arteries. The motion of the left ventricle was within normal limits with an ejection fraction of 65.5%. Coronary artery bypass graft surgery was performed on the 14th hospital day. The left internal thoracic artery was anastomosed to the LAD and saphenous vein grafts were anastomosed to the LCX and RCA, which relieved the patient's chest symptoms on exertion.

The results of the activity and gene analysis (BML Co., Ltd., Saitama, Japan) of the LDL receptor (LDLR) were as follows: the LDL-receptor activity in lymphocytes was 137% (normal rage: >80%) and none of the six common LDLR gene mutations of E119K, C317S, 1847T/C, L547V, P664L and K790X were detected.

In addition, DNA sequencing of all of the exons of LDLR and proprotein convertase subtilisin/kexin type 9 (PCSK9) did not show any gene mutations. On the other hand, sequencing of low-density lipoprotein receptor adaptor protein 1 (LDLRAP 1), which is also known as autosomal recessive hypercholesterolemia (ARH), revealed two mutations. A new DNA sequence variation in LDLRAP1 was found, as follows: 604T > C and 654A > G. The frequency of 604T > C was 0.48/0.52 and that of 654A > G was 0.50/0.50 among 31 normal control subjects. The patient had the C/C variation in 604 and the G/G variation in 654. They were both considered to be single nucleotide polymorphisms. We also sequenced the apolipoprotein B (APOB) gene. The G to A mutation at nucleotide 10,708, the major cause of mutations in familial defective APOB, was not detected using asymmetric polymerase chain reaction (PCR) (3) in this patient. The nucleotides 10,564 to 10,884 on Exon 26 of the APOB gene were sequenced in this patient and found to be normal. The sequences of the primers used in this study for sequencing LDLRAP1 (4), LDLR, PCSK9 and APOB are described in the supplementary file.

Discussion

Currently, more than 1,100 mutations occurring at different sites on the LDLR gene in patients with FH have been reported (5). It has been reported that LDLR gene mutations can be identified in 67.8% of FH patients in the Japanese population (6). In the present case, on the other hand, we were unable to identify LDLR gene mutations by screening six commonly observed sites. Patients with these six mutations comprise approximately 30% of the total number of FH heterozygotes investigated in the Japanese population (6). Taking into consideration the finding that the LDLR activity in lymphocytes was within the normal range in this patient, a nonLDLR-mediated mechanism may underlie the pathophysiology in this patient, although the possibil-

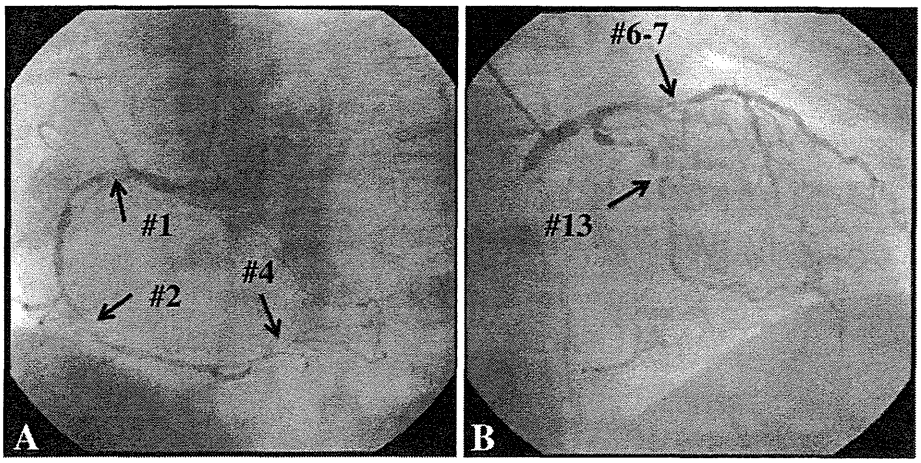

Figure 3. Coronary angiography revealed severe multivessel disease with 99% stenosis at segment (#) 1, 90% stenosis at #2, 99% stenosis at #4 of the right coronary artery (A), 90% stenosis at #6-7 of the left anterior descending artery and 99% stenosis at #13 of the left circumflex artery (B).

ity remains that a mutation of the LDLR gene other than these six mutations may have been present. However, on the other hand, compared with the LDLR gene mutation, fewer studies appear to have investigated the relationship between the LDLR genotype and its activity. A significant minority of patients (approximately 5%) who fulfill the criteria for FH with angiographically-proven coronary disease do not have a defective LDLR function or a detectable mutation in the LDLR gene (7).

Recently, several other genes that are candidates that may explain the FH phenotype have been reported, including APOB, PCSK9 and ARH (8). These nonLDLR mutations are relatively rare compared with the LDLR gene mutations whose prevalence of homozygote and heterozygote in FH are estimated to be $1/1\times10^6$ and 1/500, respectively. Additionally, the homozygote and heterozygote APOB are estimated to be $1/4\times10^6$ and 1/1,000, respectively, the heterozygote of PCSK9 is estimated to be <1/2,500 and the heterozygote of ARH is estimated to be $<1/5\times10^6$. In addition to searching for common LDLR mutations, we performed sequencing of the exons of the LDLR gene, the PCSK9 gene, the ARH gene and the APOB gene; however, no mutations that could explain the overt dyslipidemia observed in our patients were observed.

Xanthomas are a characteristic feature of FH and most usually measure a few centimeters in diameter (9). Multiple large tendinous xanthomas and advanced coronary artery atherosclerosis were noted in the present case. It has been reported that the presence of xanthomas increases the risk of cardiovascular disease in FH patients by as much as three times, suggesting that xanthomas and atherosclerosis may share a certain etiology (10). It has also been suggested that the severity of atherosclerosis and tissue lipid deposition, including the development of xanthomas and the width of the Achilles tendon, is correlated with the duration of hypercholesterolemia or the cholesterol-year score (11). It is not well known whether there is a correlation between the severity of the phenotype of FH, including multiple xanthomas and vascular diseases, and the genotype, including the sites of LDLR gene mutations. In our case, irrespective of the further extensive search for mutations in the LDLR, PCSK9, ARH and APOB genes, we were not able to identify any mutations in these genes that may potentially explain the patient's phenotype. Possible mechanisms, other than the genetic mutations examined in the current study, underlying prominent hypercholesterolemia, as observed in our patient, should be researched and identified in future studies.

The authors state that they have no Conflict of Interest (COI).

Acknowledgement

This study was partly supported by a research grant for the investigation of intractable diseases from the Ministry of Health, Labor and Welfare of Japan.

References

1. Marks D, Thorogood M, Neil HAW, Humphries SE. A review on the diagnosis, natural history, and treatment of familial hypercholesterolaemia. Atherosclerosis **168**: 1-14, 2003.
2. van Aalst-Cohen ES, Jansen AC, Tanck MW, et al. Diagnosing familial hypercholesterolaemia: the relevance of genetic testing. Eur Heart J **27**: 2240-2246, 2006.
3. Schuster H, Rauh G, Muller S, Keller C, Wolfram G, Zollner N. Allele-specific and asymmetric polymerase chain reaction amplification in combination: a one step polymerase chain reaction protocol for rapid diagnosis of familial defective apolipoprotein B-100. Analytical Biochemistry **204**: 22-25, 1992.
4. Harada K, Miyamoto Y, Morisaki H, et al. A novel Thr56Met mutation of the autosomal recessive hypercholesterolemia gene associated with hypercholesterolemia. J Atheroscler Thromb **17**: 131-140, 2010.
5. Goldstein JL, Brown MS. History of discovery: the LDL receptor. Arterioscler Thromb Vasc Biol **29**: 431-438, 2009.
6. Miyake Y, Yamamura T, Sakai N, Miyata T, Kokubo Y, Yamamoto A. Update of Japanese common LDLR gene mutations and their phenotypes. Mild type mutation L547V might predominate in the Japanese population. Atherosclerosis **203**: 153-160, 2009.
7. Sun XM, Patel DD, Knight BL, Soutar AK; the Familial Hypercholesterolaemia Regression Study Group. Comparison of the ge-

netic defect with LDL-receptor activity in cultured cells from patients with a clinical diagnosis of heterozygous familial hypercholesterolemia. Arterioscler Thromb Vasc Biol **17**: 3092-3101, 1997.

8. Rader DJ, Cohen J, Hobbs HH. Monogenic hypercholesterolemia: new insights into pathogenesis and treatment. J Clin Invest **111**: 1795-1803, 2003.

9. Weiss SW, Goldblum JR. Soft Tissue Tumors. 5th ed. Mosby Elsevier, Philadelphia, 2008: 355-358.

10. Oosterveer DM, Versmissen J, Yazdanpanah M, Hamza TH, Sijbrands EJG. Differences in characteristics and risk of cardiovascular disease in familial hypercholesterolemia patients with and without tendon xanthomas: a systematic review and meta-analysis. Atherosclerosis **207**: 311-317, 2009.

11. Schmidt HH, Hill S, Makariou EV, Feuerstein IM, Dugi KA, Hoeg JM. Relation of cholesterol-year score to severity of calcific atherosclerosis and tissue deposition in homozygous familial hypercholesterolemia. Am J Cardiol **77**: 575-580, 1996.

EUROPEAN SOCIETY OF CARDIOLOGY®

Cardiovascular Research (2013) **97**, 106–114
doi:10.1093/cvr/cvs298

Importance of endothelial NF-κB signalling in vascular remodelling and aortic aneurysm formation

Tokuo Saito[1,2†], Yutaka Hasegawa[2†], Yasushi Ishigaki[2], Tetsuya Yamada[1], Junhong Gao[1], Junta Imai[2], Kenji Uno[1], Keizo Kaneko[2], Takehide Ogihara[1], Tatsuo Shimosawa[3], Tomoichiro Asano[4], Toshiro Fujita[5], Yoshitomo Oka[2], and Hideki Katagiri[1]*

[1]Department of Metabolic Diseases, Center for Metabolic Diseases, Tohoku University Graduate School of Medicine, 2-1 Seiryo-machi, Aoba-ku, Sendai 980-8575, Japan; [2]Division of Molecular Metabolism and Diabetes, Tohoku University Graduate School of Medicine, Sendai 980-8575, Japan; [3]Department of Clinical Laboratory, Faculty of Medicine, University of Tokyo, 7-3-1 Hongo, Bunkyo-ku, Tokyo 113-8655, Japan; [4]Department of Medical Science, Graduate School of Medicine, University of Hiroshima, Hiroshima, Japan; and [5]Department of Nephrology and Endocrinology, Faculty of Medicine, University of Tokyo, 7-3-1 Hongo, Bunkyo-ku, Tokyo 113-8655, Japan

Received 30 January 2012; revised 4 September 2012; accepted 14 September 2012; online publish-ahead-of-print 26 September 2012

Time for primary review: 27 days

Aims Vascular remodelling and aortic aneurysm formation are induced mainly by inflammatory responses in the adventitia and media. However, relatively little is known about the mechanistic significance of endothelium in the pathogenesis of these vascular disorders. The transcription factor nuclear factor-kappa B (NF-κB) regulates the expressions of numerous genes, including those related to pro-inflammatory responses. Therefore, to investigate the roles of endothelial pro-inflammatory responses, we examined the impact of blocking endothelial NF-κB signalling on intimal hyperplasia and aneurysm formation.

Methods and results To block endothelial NF-κB signalling, we used transgenic mice expressing dominant-negative IκBα selectively in endothelial cells (E-DNIκB mice). E-DNIκB mice were protected from the development of cuff injury-induced neointimal formation, in association with suppressed arterial expressions of cellular adhesion molecules, a macrophage marker, and inflammatory factors. In addition, the blockade of endothelial NF-κB signalling prevented abdominal aortic aneurysm formation in an experimental model, hypercholesterolaemic apolipoprotein E-deficient mice with angiotensin II infusion. In this aneurysm model as well, aortic expressions of an adhesion molecule, a macrophage marker, and inflammatory factors were suppressed with the inhibited expression and activity of matrix metalloproteinases in the aorta.

Conclusion Endothelial NF-κB activation up-regulates adhesion molecule expression, which may trigger macrophage infiltration and inflammation in the adventitia and media. Thus, the endothelium plays important roles in vascular remodelling and aneurysm formation through its intracellular NF-κB signalling.

Keywords NF-κB • Angiotensin II • Inflammation • Atherosclerosis • Abdominal aortic aneurysm

1. Introduction

The endothelium, a single cell layer comprising the vascular wall, forms an interface between vascular structures and blood. There is growing evidence indicating the importance of the endothelium in the maintenance of vessel walls and circulatory function. Endothelial cells produce and react to a wide variety of inflammation-related mediators, including cytokines, growth factors, and adhesion molecules.[1,2] Furthermore, endothelial dysfunctions are involved in the development of many diseases, including atherosclerosis, hypertension, and other inflammatory disorders.[3] Herein, we focused on the role of the endothelium in the pathogenesis of vascular remodelling and aortic aneurysm formation, which are considered to be caused mainly by inflammatory responses in the adventitia and/or media.[4,5]

† These authors contributed equally to this work.

* Corresponding author. Tel/fax: +81 22-717-8228, Email: katagiri@med.tohoku.ac.jp

Vascular inflammation is a crucial pathological event in various vascular diseases such as angioplastic restenosis and aneurysm formation.[5–7] Intimal hyperplasia is an important feature of angioplastic restenosis and involves excessive accumulation of smooth muscle cells (SMCs) and deposition of extracellular matrix in the intimal layer. The cuff injury model is commonly used to study this type of vascular remodelling. Peri-vascular cuff placement induces adventitial inflammation, leading to medial SMC migration and resultant intimal hyperplasia.[8] Furthermore, chronic inflammation in the media and adventitia also plays a key role in the pathogenesis of aortic aneurysm.[6] A well-established model of abdominal aortic aneurysm (AAA) progression is angiotensin II (AngII) infusion into hypercholesterolaemic apoE$^{-/-}$ (apolipoprotein E-deficient) mice for 4 weeks.[9] In these mice, aneurysmal tissues were characterized by recruitment and infiltration of monocytes/macrophages, proliferation of SMCs, degradation of extra-matrix components including elastin and collagen, and increments in expressions and activities of matrix metalloproteinases (MMPs).[10] However, relatively little is known about the mechanistic importance of endothelial cells in these inflammatory lesions, such as intimal hyperplasia and AAA formation.

Herein, we investigated the roles of endothelial pro-inflammatory responses in these adventitial and medial inflammatory disorders. Nuclear factor-kappa B (NF-κB) is a transcription factor implicated in the processes of both inflammatory responses and oxidative stress.[11] NF-κB is maintained in the cytoplasm in a non-activated form by association with an inhibitor subunit, IκB, when inflammatory stimuli are absent. In response to inflammatory stimuli, proteolysis of IκB exposes a nuclear recognition site of NF-κB and then stimulates it to move into the nucleus, resulting in mRNA expressions of the genes for numerous cytokines, growth factors, and adhesion molecules.[11] We generated transgenic mice overexpressing the dominant-negative form of IκBα under the Tie2 promoter/enhancer (E-DNIκB mice). These mice exhibited functional inhibition of NF-κB signalling specifically in endothelium and prevented obesity- and age-related insulin resistance and enhanced longevity.[12] In addition, inhibition of endothelial NF-κB signalling reportedly attenuates hypertension-induced renal damage,[13] high-fat-diet-induced atherosclerosis,[14] and septic shock-induced vascular dysfunction,[15,16] indicating the pathological importance of endothelial NF-κB signalling. In the present study, using E-DNIκB mice, we examined whether and how the blockade of the NF-κB pathway in endothelial cells affects vascular remodelling and AAA formation. E-DNIκB mice are remarkably protected from the development of cuff injury-induced intimal hyperplasia as well as experimental AAA formation. Thus, the endothelium plays important roles in the promotion of vascular remodelling and aortic aneurysm formation through its intracellular NF-κB pathway.

2. Methods

2.1 Animals

All experiments were performed in conformity with the *Guide for the Care and Use of Laboratory Animals* published by the US National Institutes of Health (NIH Publication, 8th edition, 2011) and the protocols were reviewed and approved by the Institutional Committee for Use and Care of Laboratory Animals of Tohoku University, which was granted by Tohoku University Ethics Review Board (No. 76-21-66). The animals were housed in an air-conditioned environment, with a 12 h light–dark cycle. Transgenic mice (E-DNIκB mice) overexpressing the dominant-negative form of human IκBα (DNIκB), with alanine substitutions of two serine residues (32 and 36), under the Tie2 promoter/enhancer were generated and were backcrossed for at least 10 generations with C57BL/6J mice.[12]

In the experimental procedures, mice were anaesthetized by intraperitoneal injection with medetomidine (0.3 mg/kg), midazolam (4 mg/kg), and butorphanol (5 mg/kg). We added these anaesthetic agents if the mice moved to pain at operative time. We, thus, did not detect any movement of mice to pain, and their heart rate and respiratory rate were also stable during the procedures. Mice were sacrificed by cervical dislocation.

For the AAA experiments, E-DNIκB mice were crossed with apoE$^{-/-}$ mice with the C57BL/6J background[17] (The Jackson Laboratory, ME, USA) to generate E-DNIκB;apoE$^{-/-}$ mice. All experiments in this study were performed to allow comparison with littermate control mice.

2.2 Vascular injury by cuff placement around femoral arteries

Peri-vascular cuff placement surgery was carried out in male mice at 8 weeks of age as described previously.[8] After mice were anaesthetized by intraperitoneal injection with medetomidine (0.3 mg/kg), midazolam (4 mg/kg), and butorphanol (5 mg/kg), the right femoral artery was dissected from its surroundings, and vascular injury was induced by placing a 2.0 mm polyethylene PE-50 tube (inner diameter 0.58 mm; outer diameter 0.965 mm; BD Bioscience, CA, USA) around the right femoral artery. The contralateral artery served as an uninjured control. Arterial gene expressions were analysed by real-time polymerase chain reaction (RT-PCR) 7 days after cuff placement surgery. Vessels were isolated and processed for histological analysis 21 days after cuff placement surgery. The middle segment of the artery was cut at an interval of 50 μm and the areas covered by the neointima and media were quantified by Scion Image software analysis (Scion, MD, USA) of the digitized microscopic images.

2.3 Analysis and quantification of AAAs

Eight-to-16-week-old male E-DNIκB;apoE$^{-/-}$ ($n = 21$) and littermate apoE$^{-/-}$ control ($n = 20$) mice were subjected to a subcutaneous infusion of AngII (Sigma-Aldrich, MO, USA) (1000 ng/kg/min) for a period of 28 days via Alzet osmotic minipumps (model 1004; DURECT). After mice were anaesthetized by intraperitoneal injection with medetomidine (0.3 mg/kg), midazolam (4 mg/kg), and butorphanol (5 mg/kg), the minipump was implanted subcutaneously in the murine mid-scapular region through an incision in the subdorsal region.[9] The maximum width of the abdominal aorta was quantified by Scion Image software analysis. Aneurysm incidence was determined based on an increase in the external width of the suprarenal aorta of at least 50% compared with that in saline-infused mice.

2.4 Immunohistochemistry and histological analysis

For whole-body perfusion fixation with 100 mmHg pressure, the chest was opened immediately after death, and the heart punctured with a 25 gauge cannula for the infusion of phosphate-buffered saline (PBS) under physiological pressure. The blood was drained through an incision of the inferior vena cava. After 5 min, PBS was replaced with 10% buffered formaldehyde and the mice perfused for an additional 5 min prior to dissection and overnight post-fixation with 10% buffered formaldehyde. Tissues were dehydrated through various concentrations of ethanol and embedded in paraffin as described previously.[18] Excised whole and thoracic aortae and femoral arterial tissues were subjected to staining with elastica and haematoxylin–eosin and immunostaining with antibodies against Mac-3 (BD Bioscience) or the p65 subunit of NF-κB (Santa Cruz Biotechnology, CA, USA) as described previously.[18] The areas of the intima and media were measured and averaged in five cross-sections per mouse.

2.5 Blood analysis

Blood glucose, plasma insulin, total cholesterol, and triglyceride concentrations were determined as described previously.[19] Plasma thiobarbituric acid-reactive substance (TBARS) levels were measured with a TBARS Assay Kit (Cayman Chemical Co., MN, USA).

2.6 Blood pressure measurement

Systolic blood pressure in the conscious state was measured by the indirect tail cuff method, using a model MK-2000 BP monitor for mice and rats (Muromachi Kikai, Tokyo, Japan) as described previously.[20] At least six readings were obtained for each experiment, and a mean value was assigned to male E-DNIκB;apoE$^{-/-}$ ($n = 13$) and littermate control apoE$^{-/-}$ ($n = 11$) mice.

2.7 Gelatin zymography

Aortic proteins were extracted using a gelatin-zymography kit (Primary Cell, Sapporo, Japan) as previously described.[10] The molecular sizes of gelatinolytic activities were determined according to the manufacturer's instructions. The sum of MMP-2 and Pro-MMP-2 was measured as total MMP-2 activity.

2.8 Quantitative RT-PCR-based gene expressions

Whole aortae and femoral arteries were perfused and rinsed with physiological saline. Total RNA was extracted using an RNAeasy micro kit (Qiagen, CA, USA). Quantitative RT-PCR was performed as previously described.[18] cDNA synthesis was performed with a Cloned AMV First Strand Synthesis Kit (Invitrogen, CA, USA), using 1.0 μg of total RNA. cDNA synthesized from total RNA was evaluated using a quantitative RT-PCR system (Light Cycler Quick System 350S; Roche Diagnostics GmbH). The relative amounts of mRNA were calculated with β-actin mRNA as the invariant control. The oligonucleotide primers are described in Supplementary material online, *Table S1*.

2.9 Statistical analysis

Data are expressed as means ± SEM. All statistical analyses were performed with the Ekuseru-Tokei 2010 statistical software (Social Survey Research Information Co., Ltd, Tokyo, Japan). All data were tested for normality by the Kolmogorov–Smirnov test. When data were normally distributed, the statistical significance of differences was assessed with one-way ANOVA. The Mann–Whitney *U* test was applied when data were not normally distributed. *P*-values of <0.05 were considered to be statistically significant.

3. Results

3.1 Cuff injury-induced intimal hyperplasia was suppressed in E-DNIκB mice

To elucidate the roles of endothelial NF-κB signalling in vascular remodelling, we examined cuff injury-induced intimal hyperplasia in E-DNIκB mice, i.e. transgenic mice overexpressing the dominant-negative form of IκBα under the Tie2 promoter/enhancer.[12] As reported previously,[12] immunoblotting revealed no detectable expression of the dominant-negative form of IκBα in macrophages, whereas it was clearly detected in the aorta and lung in which the endothelium is abundant (see Supplementary material online, *Figure S1*). Endogenous IκBα proteins in the lung were degraded after TNF-α stimulation in a dose-dependent manner, whereas DNIκBα remained essentially intact without degradation after TNF-α stimulation (see Supplementary material online, *Figure S2A*). In addition, TNF-α-stimulated up-regulation of VCAM-1 in endothelial cells was markedly suppressed in E-DNIκB mice compared with the wild-type controls (see Supplementary material online, *Figure S2B*). In contrast, TNF-α stimulation similarly up-regulated interleukin (IL)-6, a target gene of NF-κB, in peritoneal macrophages isolated from the wild-type and E-DNIκB mice (see Supplementary material online, *Figure S2C*). These findings demonstrate the functional blockade of NF-κB signalling selectively in endothelial cells of the E-DNIκB mice used in this study.

E-DNIκB mice showed no obvious differences in metabolism from control mice under normal chow-fed conditions. At 8 weeks of age, body weights, fasting blood glucose, and insulin levels were similar in E-DNIκB mice and their wild-type littermates. Neither total cholesterol nor triglyceride levels differed significantly between the two. In addition, blood pressures were similar in these two groups of mice (see Supplementary material online, *Table S2*). Under these conditions, a peri-vascular cuff was placed around the femoral artery, followed by examination of morphometric changes in the artery after 21 days.

No apparent histological differences were observed in uninjured femoral arteries between E-DNIκB and wild-type littermate mice (*Figure 1A*). In contrast, in cuff-injured femoral arteries, E-DNIκB mice exhibited apparent suppression of intimal hyperplasia (*Figure 1A*). Intimal hyperplasia, when quantified as the intimal area and intima/media ratio, was also significantly decreased (by 44.5 and 47.5%, respectively) in E-DNIκB mice compared with littermate controls (*Figure 1B* and *C*). Thus, the blockade of endothelial NF-κB signalling suppressed vascular remodelling.

3.2 Endothelial NF-κB blockade suppressed gene expressions of inflammation- and SMC proliferation-related factors

Intimal hyperplasia in the arterial wall is reportedly attributable to increased inflammatory reactions induced by interactions between recruited leucocytes and migrating SMCs.[21] Therefore, we next examined local expressions of genes related to vascular remodelling in cuff-injured femoral arteries 7 days after cuff placement. In cuff-injured femoral arteries, expressions of inflammatory factors, such as monocyte chemoattractant protein-1 (MCP-1), TNF-α, IL-1β, and IL-6, were markedly suppressed in E-DNIκB mice compared with controls (*Figure 2A*), suggesting suppressed arterial inflammation. Compatible with this notion, arterial expression of F4/80, a macrophage marker, was significantly decreased in E-DNIκB (*Figure 2B*). In addition, endothelial DNIκB expression inhibited expressions of vascular SMC proliferation-related factors, such as platelet-derived growth factor-B and stromal cell-derived factor-1α (also known as CXCL12) (*Figure 2C*). These findings suggest cuff injury-induced inflammation and SMC proliferation to be suppressed in E-DNIκB mice. Furthermore, arterial expressions of cellular adhesion molecules, such as VCAM-1 and ICAM-1, were remarkably decreased in E-DNIκB mice (*Figure 2D*). Anti-oxidant enzymes, such as manganese superoxide dismutase (MnSOD) and glutathione-*S*-transferase (GST), which are up-regulated in response to oxidative stress, were attenuated by endothelial DNIκB expression (*Figure 2E*). These findings suggest that the blockade of NF-κB signalling in the endothelium inhibits up-regulation of vascular adhesion molecules and the resultant

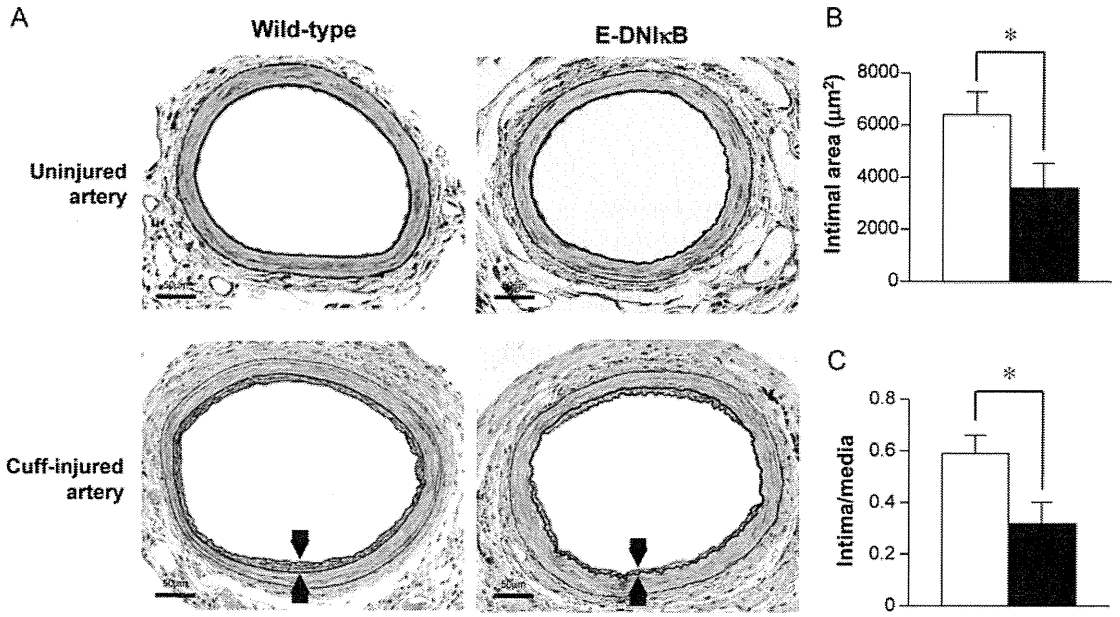

Figure 1 Cuff injury-induced intimal hyperplasia was inhibited in E-DNIκB mice. Peri-vascular cuff placement surgery was carried out on male E-DNIκB and littermate wild-type mice at 8 weeks of age, followed by histological analysis after 21 days. (*A*) Representative histological findings of uninjured (upper) and cuff-injured (lower) femoral arteries from wild-type (left) and E-DNIκB (right) mice. Magnification: ×200. Scale bars indicate 50 μm. Arrows indicate the intimal hyperplasia induced by cuff injury. (*B*) Intimal area of cuff-injured femoral arteries of wild-type (white bar, $n = 6$) and E-DNIκB (black bar, $n = 4$) mice. (*C*) Intimal-to-medial area ratios of cuff-injured femoral arteries of wild-type (white bar, $n = 6$) and E-DNIκB (black bar, $n = 4$) mice. Data are presented as means ± SEM. *$P < 0.05$, assessed by one-way ANOVA.

macrophage infiltration, which is the mechanism underlying suppression of cuff injury-induced adventitial inflammation.

3.3 E-DNIκB mice were protected from experimental AAA formation

In the cuff injury model, adventitial inflammation is considered to be a major cause of medial SMC migration to the subendothelial space.[22] We next examined the contribution of NF-κB signalling in the endothelium to aneurysm formation, another aortic medial and adventitial lesion. E-DNIκB mice were crossed with apoE$^{-/-}$ mice, resulting in the generation of E-DNIκB;apoE$^{-/-}$ mice. E-DNIκB;apoE$^{-/-}$ mice and control apoE$^{-/-}$ mice were started on a 28-day AngII infusion (1000 ng/kg/min), followed by abdominal aorta analyses.

Body weight, blood glucose and serum levels of insulin, triglycerides, and total cholesterol were similar in E-DNIκB;apoE$^{-/-}$ mice and control apoE$^{-/-}$ mice after the 28-day AngII infusion (see Supplementary material online, *Table S3*). Although systolic blood pressure was significantly elevated in control apoE$^{-/-}$ mice, blood pressure elevation was blocked by endothelial DNIκB expression (*Figure 3A*). Notably, AAA formation after AngII infusion was attenuated in E-DNIκB;apoE$^{-/-}$ mice compared with control apoE$^{-/-}$ mice (*Figure 3B*). AngII infusion for 28 days led to AAA formation at an incidence of 85.0% (17 out of 20) in control apoE$^{-/-}$ mice, whereas AAA was detected in only 19.0% (4 out of 21) of E-DNIκB;apoE$^{-/-}$ mice. The maximal abdominal aortic diameter of E-DNIκB;apoE$^{-/-}$ mice (2.06 ± 0.22 mm) was significantly decreased compared with that of control apoE$^{-/-}$ mice (1.49 ± 0.08 mm) (*Figure 3C*). Thus, the blockade of endothelial NF-κB signalling clearly prevented AAA progression in this experimental model of AngII infusion into hypercholesterolaemic mice.

3.4 AngII-induced macrophage infiltration, aortic inflammation, and oxidative stress were markedly reduced by blockade of NF-κB signalling in endothelial cells

To further delineate the effects of the endothelial NF-κB blockade on AAA formation, we next performed morphological and immunohistochemical studies of vessel-wall constituents. Cross-sectional histology with elastica and haematoxylin–eosin staining revealed that AngII-induced lumen dilatation and medial elastin breaks, which were observed in the abdominal aortae in apoE$^{-/-}$ controls, were remarkably attenuated in the aortae in E-DNIκB;apoE$^{-/-}$ mice (*Figure 4A*). Furthermore, immunohistochemistry with anti-Mac-3 also revealed massive infiltration of macrophages in the media and adventitia of the aortic walls of apoE$^{-/-}$ controls, whereas macrophage infiltration was markedly inhibited in E-DNIκB;apoE$^{-/-}$ mice (*Figure 4B*).

These findings were compatible with aortic gene expressions. Aortic F4/80 expression was significantly decreased in E-DNIκB;apoE$^{-/-}$ mice (*Figure 5A*). In addition, aortic expressions of inflammatory factors, such as MCP-1 and IL-1β (*Figure 5B*), and the cellular adhesion molecule VCAM-1 (*Figure 5C*) were significantly decreased in E-DNIκB;apoE$^{-/-}$ mice. Furthermore, an anti-oxidant enzyme MnSOD tended to be decreased and GST was markedly suppressed (*Figure 5D*), suggesting decreased oxidative stress. Supporting this notion, plasma levels of TBARS, a marker of oxidative stress, were significantly decreased in E-DNIκB;apoE$^{-/-}$ mice (*Figure 5E*). Thus, oxidative stress in the aorta

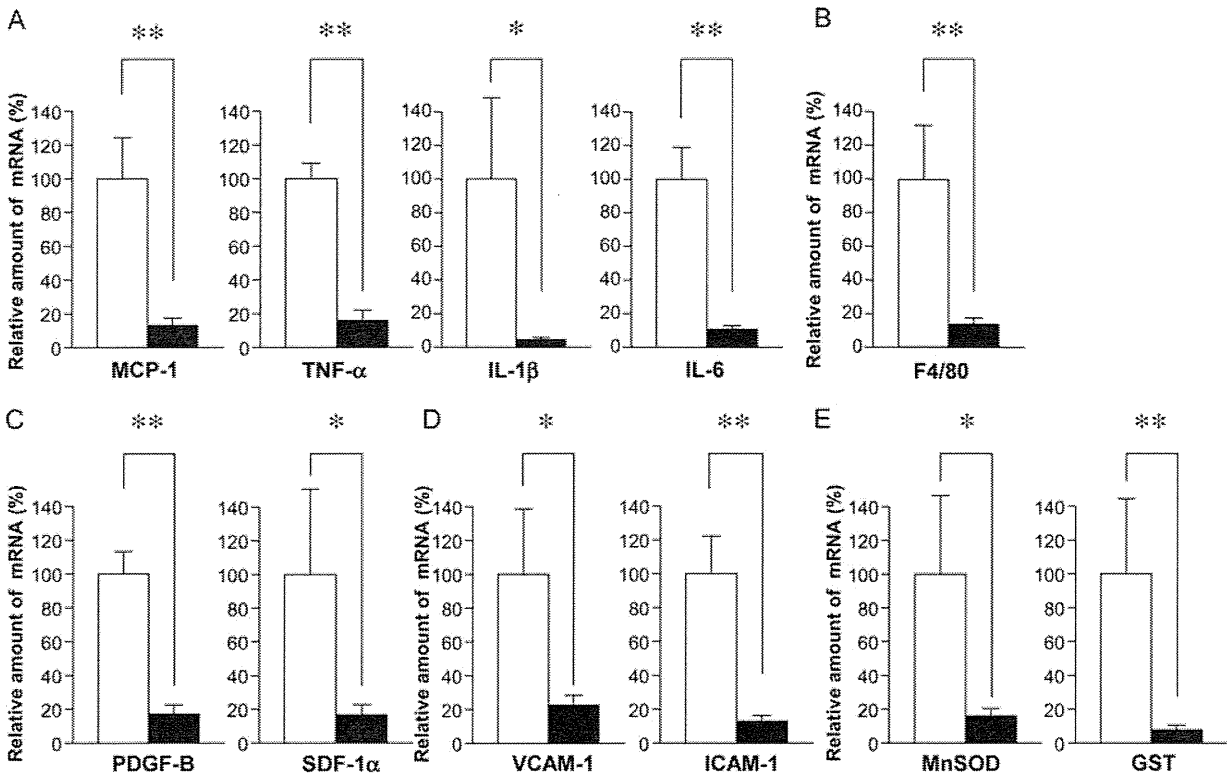

Figure 2 Expressions of inflammation- and SMC proliferation-related factors and adhesion molecules in cuff-injured arteries were suppressed in E-DNIκB mice. Arterial expressions of pro-inflammatory cytokines (*A*), a macrophage marker (*B*), vascular SMC proliferation-related factors (*C*), cellular adhesion molecules (*D*), and anti-oxidant enzymes (*E*) were quantified by RT-PCR 7 days after cuff placement in wild-type (white bars, $n = 6$) and E-DNIκB (black bars, $n = 6$) mice. Data are presented as means ± SEM. $^{*}P < 0.05$, $^{**}P < 0.01$, assessed by one-way ANOVA.

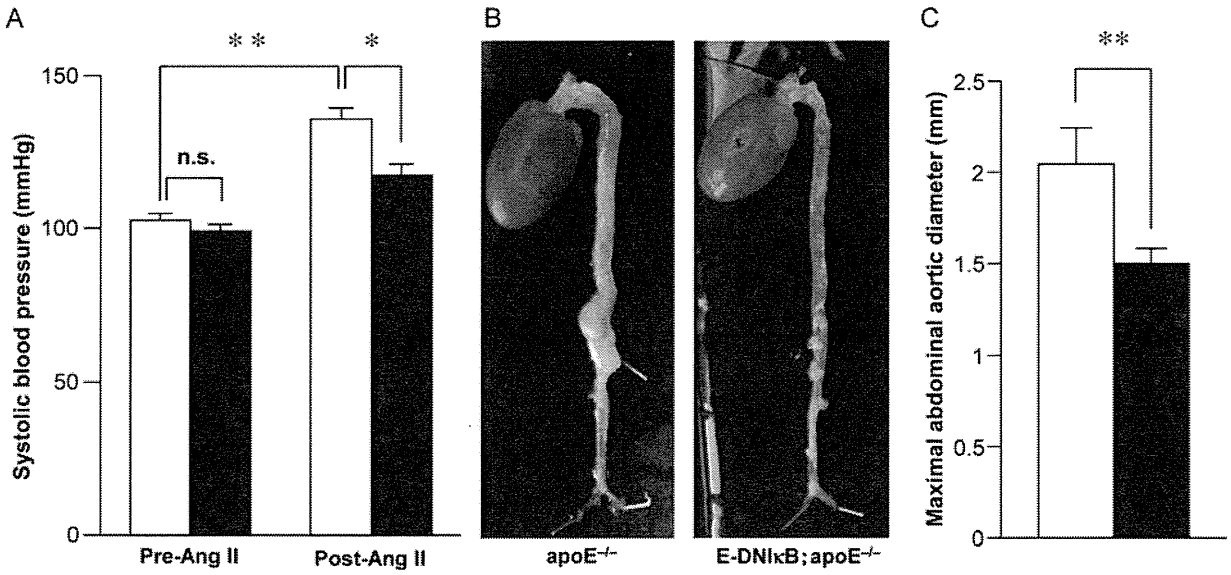

Figure 3 AAA formation was inhibited by the blockade of endothelial NF-κB signalling. E-DNIκB;apoE$^{-/-}$ (black bars, $n = 21$) and littermate apoE$^{-/-}$ control (white bars, $n = 20$) mice were subjected to a subcutaneous infusion of AngII for 28 days. (*A*) Systolic blood pressures of control apoE$^{-/-}$ (white bars, $n = 11$) and E-DNIκB;apoE$^{-/-}$ (black bars, $n = 13$) mice before and after 4-week AngII infusion. (*B*) Representative macroscopic findings of the abdominal aortae from control apoE$^{-/-}$ (left) and E-DNIκB;apoE$^{-/-}$ (right) mice. (*C*) Maximal abdominal aortic diameters from control apoE$^{-/-}$ mice and E-DNIB;apoE$^{-/-}$ mice. Data are presented as means ± SEM. $^{*}P < 0.05$, $^{**}P < 0.01$, assessed by one-way ANOVA.

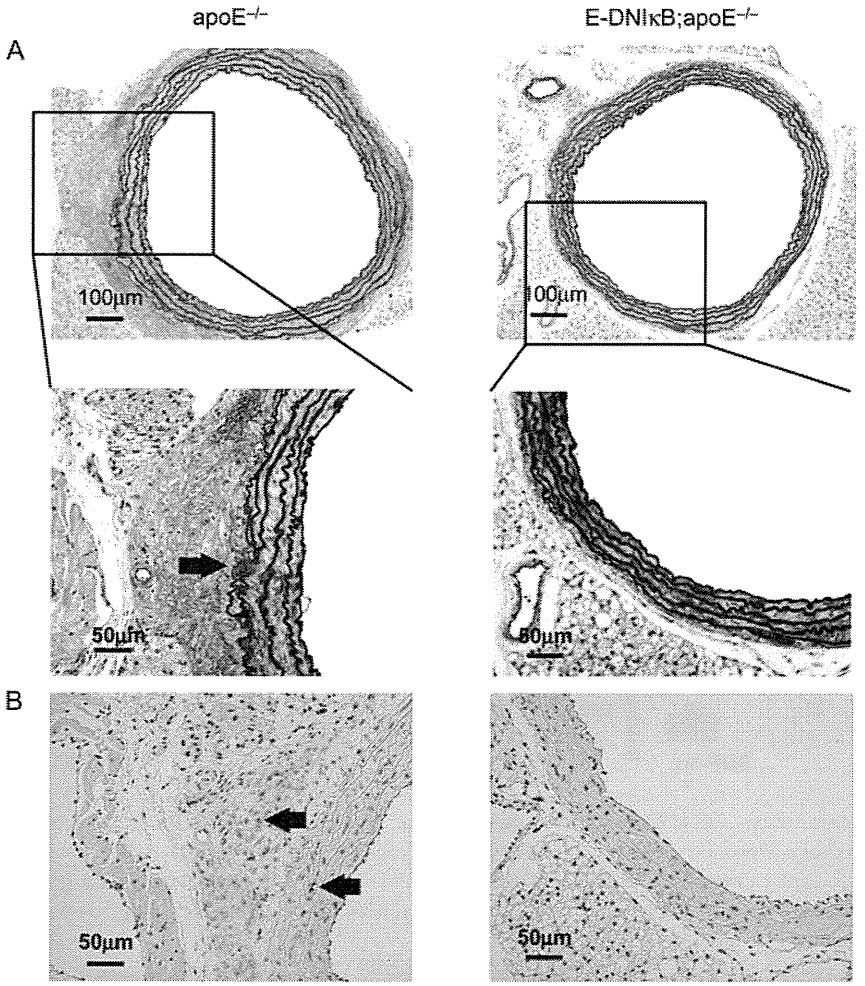

Figure 4 Medial elastin breaks and macrophage infiltration were markedly inhibited by the blockade of endothelial NF-κB signalling. E-DNIκB;apoE$^{-/-}$ and littermate apoE$^{-/-}$ control mice were subjected to a subcutaneous infusion of AngII for 28 days. (*A*) Aortic sections were counterstained with elastica and haematoxylin–eosin. The arrow indicates breaks in the elastic fibres of apoE$^{-/-}$ control mice. Magnification: (*A* upper): ×100; (*A* lower): ×200. (*B*) Aortic sections were immunostained with anti-mac3 antibody. Magnification: ×200. The arrows indicate Mac 3-positive cells. Results are representative of data obtained from six mice per group.

as well as the whole body was decreased in E-DNIκB;apoE$^{-/-}$ mice. Therefore, the blockade of NF-κB signalling in endothelial cells alone has a strong inhibitory impact on macrophage infiltration, aortic inflammation, and oxidative stress, thereby preventing aortic aneurysm formation.

3.5 Activation and expression of MMPs were inhibited in the aortae of E-DNIκB;apoE$^{-/-}$ mice

MMPs, which are zinc-dependent endopeptidases, have been shown to be responsible for the destruction of the orderly elastin and collagen network of the aorta.[23] In fact, activated MMP-2 and MMP-9 levels are reportedly elevated in human AAA tissue.[10] Macrophage-derived MMP-9 and SMC-derived MMP-2 are reportedly both required and work in concert, resulting in aneurysm progression.[10] Therefore, we next analysed the activities of aortic MMP-2 and MMP-9 by the gelatin zymography technique. The AngII-induced activities of aortic MMP-2 and pro-MMP-2, as well as those of pro-MMP-9, were markedly suppressed in E-DNIκB;apoE$^{-/-}$ mice compared with control apoE$^{-/-}$ mice (*Figure 6A*). RT-PCR revealed that expressions of MMP-2 and MMP-9 were decreased (*Figure 6B*). Thus, decreased MMP-2 and MMP-9 expressions/activities are involved in the reduced incidence and severity of experimental aneurysm formation observed in E-DNIκB;apoE$^{-/-}$ mice.

4. Discussion

To investigate the roles of endothelial pro-inflammatory responses in adventitial and medial inflammatory disorders, we used E-DNIκB mice in the present study. We previously reported that, in E-DNIκB mice, DNIκBα was selectively expressed in endothelial cells and resistant to degradation, thereby inhibiting the movement of NF-κB to the nucleus even after TNF-α stimulation.[12] Furthermore, pro-inflammatory responses were suppressed in endothelial cells, but not in circulating cells, obtained from E-DNIκB mice.[12] Although only a small fraction of the circulating leucocytes and marrow cells were reported

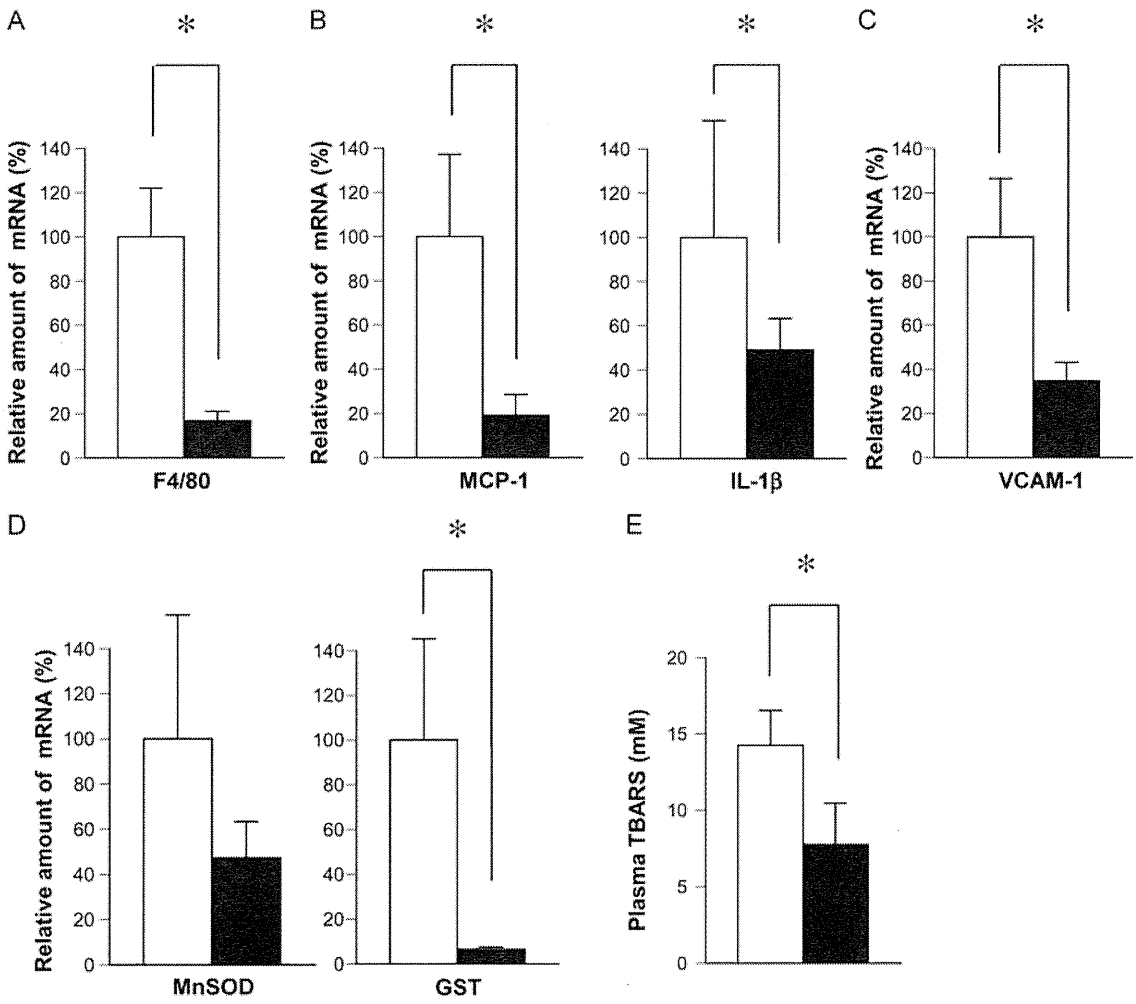

Figure 5 Suppression of inflammation and oxidative stress by the blockade of endothelial NF-κB signalling. (*A–D*) Aortic expressions of a macrophage marker (*A*), pro-inflammatory cytokines (*B*), a cellular adhesion molecule (*C*), and anti-oxidant enzymes (*D*) were quantified by RT-PCR after 28-day AngII infusions into apoE$^{-/-}$ control (white bars) and E-DNIκB;apoE$^{-/-}$ (black bars, $n = 5–6$ per group) mice. (*E*) Plasma TBARS concentrations were measured in control apoE$^{-/-}$ and E-DNIκB;apoE$^{-/-}$ mice. Data are presented as means ± SEM. *$P < 0.05$, assessed by one-way ANOVA.

to weakly express the Tie2/Tek gene,[24] Tie2-expressing monocytes, including macrophages, are preferentially extravasate in tumours and regenerating tissues. In our models, DNIκBα was not detected by immunoblotting in isolated peritoneal macrophages. In addition, macrophages from E-DNIκB mice did not suppress TNF-α-stimulated expression of IL-6, a target gene of NF-κB. Although we cannot completely rule out that a very small amount of DNIκB was expressed in macrophages or other circulating cells, these data suggest that NF-κB signalling is functionally blocked selectively in endothelial cells of the E-DNIκB mice used in this study and that effects of DNIκB in non-endothelial cells, if even present, were very small.

The first important result obtained in this study is that the endothelial blockade of intracellular NF-κB signalling markedly suppressed intimal hyperplasia. Peri-vascular cuff placement stimulates arteries from outside of the adventitia and the resultant adventitial inflammatory cell infiltration is considered to cause migration and accumulation of medial SMCs.[4] In the present study, interestingly, the blockade of NF-κB signalling only in the endothelium suppressed these adventitial and medial events. In the peri-vascular cuff-injured arteries of E-DNIκB mice, expressions of endothelial adhesion molecules, such as VCAM-1 and ICAM-1, were markedly decreased, in association with reduced macrophage marker expression. Thus, the endothelium-macrophage interaction, triggered by endothelial adhesion molecules, was markedly inhibited in E-DNIκB mice, which is likely involved in the mechanism underlying suppression of adventitial inflammation and the resultant vascular remodelling. Therefore, up-regulation of cellular adhesion molecules in the endothelium is likely to be the early important event in cuff injury-induced vascular remodelling, and this step appears to be regulated by NF-κB signalling in endothelial cells. Thus, the endothelium, which lines the entire vascular system in a single cell layer, may play important roles in inflammatory responses, thereby inducing vascular remodelling. In addition to the arterial lumen, the adventitial vasa vasorum, which is enriched in the endothelium, acts as a conduit for the entry of inflammatory mediators and circulating cells into the vessel wall. Growing evidence supports the 'outside–in' theory, in which vascular inflammation is initiated in the adventitia and progresses inward towards the intima.[25] The blockade of NF-κB signalling in the adventitial vasa

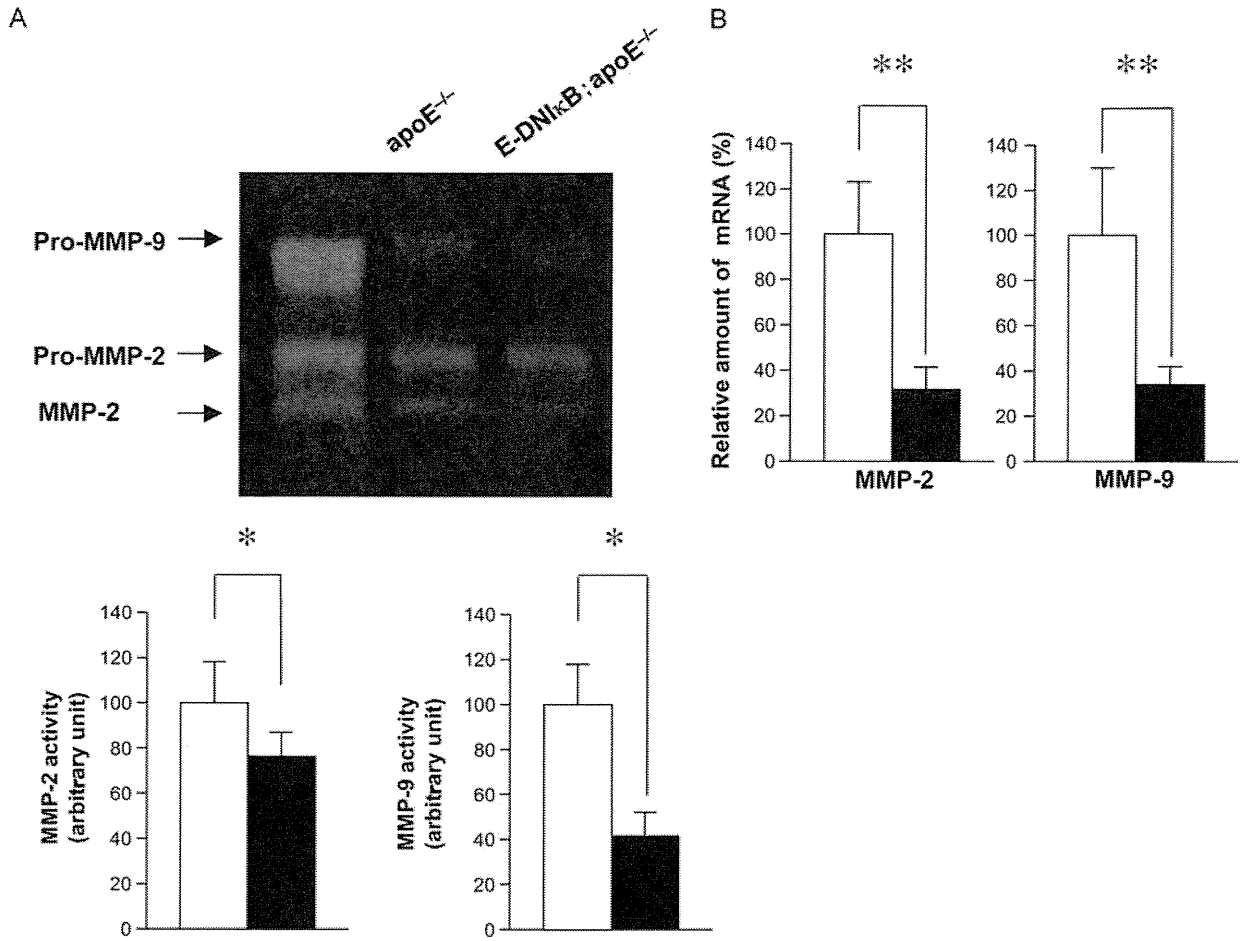

Figure 6 Suppression of MMP activation by the blockade of endothelial NF-κB signalling. (*A*) Representative zymographic analyses for MMP activities in aortae from control apoE$^{-/-}$ and E-DNIκB;apoE$^{-/-}$ mice. Markers for MMP-2, pro-MMP-2 and pro-MMP-9 are shown in the left lane. Gelatin zymographic activities of MMP-2 and MMP-9 in aortae from control apoE$^{-/-}$ and E-DNIκB;apoE$^{-/-}$ mice were quantified by densitometric analysis. (*B*) Aortic expressions of MMP-2 and MMP-9 were quantified by RT-PCR after 28-day AngII infusions into apoE$^{-/-}$ control (white bars, $n = 6$) and E-DNIκB;apoE$^{-/-}$ (black bars, $n = 8$) mice. Relative amounts of mRNA in aortae from control apoE$^{-/-}$ and E-DNIκB;apoE$^{-/-}$ mice. Data are presented as means ± SEM. *$P < 0.05$, **$P < 0.01$, assessed by one-way ANOVA.

vasorum endothelium might inhibit the entry of macrophages and inflammatory mediators, thereby contributing to the vascular remodelling suppression observed in E-DNIκB mice.

Another important finding of the present study is that NF-κB signalling in the endothelium is the key step in aortic aneurysm formation. Aneurysm formation is mainly influenced by the physical and biochemical vascular inflammatory responses in the media and adventitia through several mechanisms.[6] Infiltrating macrophages/leucocytes are major sources of proteinases, such as MMPs, that degrade structural proteins, including elastin, collagen, and laminin, thereby weakening the aortic wall.[6,10] In addition, infiltrating immune cells may exacerbate tissue injury through the release of inflammatory cytokines, leading to further recruitment of immune cells and induction of SMC apoptosis.[26] Apoptotic SMCs play major roles in aortic extracellular matrix production as well as additional protease release, contributing to matrix degradation.[10,26] In addition, oxidative stress is reportedly involved in aneurysm progression.[27] In the present study, the blockade of endothelial NF-κB signalling suppressed aortic expressions of inflammatory factors and oxidative stress markers in an experimental AAA model. In addition, VCAM-1 and F4/80 expressions were markedly decreased in the aortae of E-DNIκB;apoE$^{-/-}$ mice, indicating the suppression of the endothelium–leucocyte interaction. Thus, endothelial NF-κB activation may induce the endothelium–leucocyte interaction, triggering whole-aorta inflammation. Furthermore, aortic expressions and activations of MMP-2 and MMP-9 were also inhibited by the endothelial blockade of NF-κB signalling. These findings, taken together, suggest that the endothelial pro-inflammatory response is a major early event in aortic aneurysm formation. This notion that the endothelium–leucocyte interaction triggers AAA formation is supported by previous reports indicating that global P-selectin deficiency and haematopoietic CCR2 deficiency attenuate experimental aortic aneurysm formation.[28,29]

AngII reportedly induces intracellular NF-κB activation.[30] However, although a growing body of evidence has accumulated regarding AngII signalling in SMCs, much less is known about endothelial AngII signal transduction and function.[31] The present study shows the specific importance of the endothelium, which eventually modulates inflammation in the adventitia and media, through intracellular NF-κB

signalling. Furthermore, AngII-induced elevation of blood pressure was almost completely absent in E-DNIκB;apoE$^{-/-}$ mice, suggesting that endothelial NF-κB activation mediates AngII-related hypertension. Thus, NF-κB signalling in the endothelium plays mechanistic roles in various aspects of the development of vascular disorders. Since cohort and epidemiological studies have revealed the relevance of hypertension to AAA,[32] this preventive effect on blood pressure elevation might participate in the suppression of AAA formation observed in E-DNIκB;apoE$^{-/-}$ mice. However, Cassis *et al.* [33] recently reported based on the three data sets described below that blood pressure elevation *per se* is not a major determinant of AAA formation in this model. Blood pressure elevation in apoE$^{-/-}$ mice infused with norepinephrine did not induce AAA formation. Subpressor infusion of AngII induced AAA development in apoE$^{-/-}$ mice. Furthermore, lowering systolic blood pressure by the administration of hydralazine to AngII-infused apoE$^{-/-}$ mice did not prevent AAA formation. Thus, the suppression of inflammatory responses, rather than the prevention of hypertension, is likely to be the main contributor to preventive effects of the endothelial NF-κB blockade on AAA formation.

In conclusion, this study provides strong evidence of the major impact of the endothelium on vascular remodelling and AAA formation through intracellular NF-κB signalling. Endothelial NF-κB signalling up-regulates adhesion molecules, triggering macrophage infiltration and the resultant vascular inflammation in the adventitia and media. Therefore, NF-κB activation is a major early event in the pathogenesis of these inflammation-related vascular diseases, making the blockade of endothelial NF-κB signalling a promising strategy for preventing vascular inflammation and dysfunction, especially aneurysm formation as well as angioplastic restenosis.

Supplementary material

Supplementary material is available at *Cardiovascular Research* online.

Acknowledgements

We thank Ms I. Sato, J. Fushimi, K. Kawamura, M. Aizawa, M. Hoshi, and T. Takasugi for their technical support. We also appreciate the useful guidance from Dr Morita and Ms Tatebe in the cuff injury experiments.

Conflict of interest: none declared.

Funding

This work was supported by the Japan Society for the Promotion of Science (Grants-in-Aid for Scientific Research 15390282 to H.K. and 22790681 to Y.H.). This work was also supported by the Ministry of Education, Culture, Sports, Science and Technology of Japan (a Grant-in-Aid for Scientific Research on Innovative Areas to H.K. and the Global-COE to H.K. and Y.O.).

References

1. Aird WC. Phenotypic heterogeneity of the endothelium. I. Structure, function, and mechanisms. *Circ Res* 2007;**100**:158–173.
2. Aird WC. Phenotypic heterogeneity of the endothelium. II. Representative vascular beds. *Circ Res* 2007;**100**:174–190.
3. Kim JA, Montagnani M, Koh KK, Quon MJ. Reciprocal relationships between insulin resistance and endothelial dysfunction: molecular and pathophysiological mechanisms. *Circulation* 2006;**113**:1888–1904.
4. Kockx MM, De Meyer GR, Jacob WA, Bult H, Herman AG. Triphasic sequence of neointimal formation in the cuffed carotid artery of the rabbit. *Arterioscler Thromb* 1992;**12**:1447–1457.
5. Golledge J, Muller J, Daugherty A, Norman P. Abdominal aortic aneurysm: pathogenesis and implications for management. *Arterioscler Thromb Vasc Biol* 2006;**26**:2605–2613.
6. Shimizu K, Mitchell RN, Libby P. Inflammation and cellular immune responses in abdominal aortic aneurysms. *Arterioscler Thromb Vasc Biol* 2006;**26**:987–994.
7. Rocha VZ, Libby P. Obesity, inflammation, and atherosclerosis. *Nat Rev Cardiol* 2009;**6**:399–409.
8. Gao J, Ishigaki Y, Yamada T, Kondo K, Yamaguchi S, Imai J *et al.* Involvement of endoplasmic stress protein C/EBP homologous protein in arteriosclerosis acceleration with augmented biological stress responses. *Circulation* 2011;**124**:830–839.
9. Daugherty A, Manning MW, Cassis LA. Angiotensin II promotes atherosclerotic lesions and aneurysms in apolipoprotein E-deficient mice. *J Clin Invest* 2000;**105**:1605–1612.
10. Longo GM, Xiong W, Greiner TC, Zhao Y, Fiotti N, Baxter BT. Matrix metalloproteinases 2 and 9 work in concert to produce aortic aneurysms. *J Clin Invest* 2002;**110**:625–632.
11. Hayden MS, Ghosh S. Shared principles in NF-kappaB signaling. *Cell* 2008;**132**:344–362.
12. Hasegawa Y, Ogihara T, Yamada T, Ishigaki Y, Imai J, Uno K *et al.* Bone marrow (BM) transplantation promotes beta-cell regeneration after acute injury through BM cell mobilization. *Endocrinology* 2007;**148**:2006–2015.
13. Henke N, Schmidt-Ullrich R, Dechend R, Park JK, Qadri F, Wellner M *et al.* Vascular endothelial cell-specific NF-kappaB suppression attenuates hypertension-induced renal damage. *Circ Res* 2007;**101**:268–276.
14. Gareus R, Kotsaki E, Xanthoulea S, van der Made I, Gijbels MJ, Kardakaris R *et al.* Endothelial cell-specific NF-kappaB inhibition protects mice from atherosclerosis. *Cell Metab* 2008;**8**:372–383.
15. Ye X, Ding J, Zhou X, Chen G, Liu SF. Divergent roles of endothelial NF-kappaB in multiple organ injury and bacterial clearance in mouse models of sepsis. *J Exp Med* 2008;**205**:1303–1315.
16. Ding J, Song D, Ye X, Liu SF. A pivotal role of endothelial-specific NF-{kappa}B signaling in the pathogenesis of septic shock and septic vascular dysfunction. *J Immunol* 2009;**183**:4031–4038.
17. Zhang SH, Reddick RL, Piedrahita JA, Maeda N. Spontaneous hypercholesterolemia and arterial lesions in mice lacking apolipoprotein E. *Science* 1992;**258**:468–471.
18. Ishigaki Y, Katagiri H, Gao J, Yamada T, Imai J, Uno K *et al.* Impact of plasma oxidized low-density lipoprotein removal on atherosclerosis. *Circulation* 2008;**118**:75–83.
19. Ishigaki Y, Katagiri H, Yamada T, Ogihara T, Imai J, Uno K *et al.* Dissipating excess energy stored in the liver is a potential treatment strategy for diabetes associated with obesity. *Diabetes* 2005;**54**:322–332.
20. Gao J, Katagiri H, Ishigaki Y, Yamada T, Ogihara T, Imai J *et al.* Involvement of apolipoprotein E in excess fat accumulation and insulin resistance. *Diabetes* 2007;**56**:24–33.
21. Libby P. Inflammation in atherosclerosis. *Nature* 2002;**420**:868–874.
22. Egashira K, Zhao Q, Kataoka C, Ohtani K, Usui M, Charo IF *et al.* Importance of monocyte chemoattractant protein-1 pathway in neointimal hyperplasia after periarterial injury in mice and monkeys. *Circ Res* 2002;**90**:1167–1172.
23. Hellenthal FA, Buurman WA, Wodzig WK, Schurink GW. Biomarkers of AAA progression. Part 1: extracellular matrix degeneration. *Nat Rev Cardiol* 2009;**6**:464–474.
24. De Palma M, Venneri MA, Roca C, Naldini L. Targeting exogenous genes to tumor angiogenesis by transplantation of genetically modified hematopoietic stem cells. *Nat Med* 2003;**9**:789–795.
25. Maiellaro K, Taylor WR. The role of the adventitia in vascular inflammation. *Cardiovasc Res* 2007;**75**:640–648.
26. Henderson EL, Geng YJ, Sukhova GK, Whittemore AD, Knox J, Libby P. Death of smooth muscle cells and expression of mediators of apoptosis by T lymphocytes in human abdominal aortic aneurysms. *Circulation* 1999;**99**:96–104.
27. McCormick ML, Gavrila D, Weintraub NL. Role of oxidative stress in the pathogenesis of abdominal aortic aneurysms. *Arterioscler Thromb Vasc Biol* 2007;**27**:461–469.
28. Hannawa KK, Cho BS, Sinha I, Roelofs KJ, Myers DD, Wakefield TJ *et al.* Attenuation of experimental aortic aneurysm formation in P-selectin knockout mice. *Ann NY Acad Sci* 2006;**1085**:353–359.
29. Ishibashi M, Egashira K, Zhao Q, Hiasa K, Ohtani K, Ihara Y *et al.* Bone marrow-derived monocyte chemoattractant protein-1 receptor CCR2 is critical in angiotensin II-induced acceleration of atherosclerosis and aneurysm formation in hypercholesterolemic mice. *Arterioscler Thromb Vasc Biol* 2004;**24**:e174–e178.
30. Tham DM, Martin-McNulty B, Wang YX, Wilson DW, Vergona R, Sullivan ME *et al.* Angiotensin II is associated with activation of NF-kappaB-mediated genes and down-regulation of PPARs. *Physiol Genomics* 2002;**11**:21–30.
31. Higuchi S, Ohtsu H, Suzuki H, Shirai H, Frank GD, Eguchi S. Angiotensin II signal transduction through the AT1 receptor: novel insights into mechanisms and pathophysiology. *Clin Sci* 2007;**112**:417–428.
32. van der Vliet JA, Boll AP. Abdominal aortic aneurysm. *Lancet* 1997;**349**:863–866.
33. Cassis LA, Gupte M, Thayer S, Zhang X, Charnigo R, Howatt DA *et al.* ANG II infusion promotes abdominal aortic aneurysms independent of increased blood pressure in hypercholesterolemic mice. *Am J Physiol Heart Circ Physiol* 2009;**296**:1660–1665.

Am J Physiol Endocrinol Metab 304: E301–E309, 2013.
First published December 4, 2012; doi:10.1152/ajpendo.00388.2012.

Chronic mild stress alters circadian expressions of molecular clock genes in the liver

Kei Takahashi,[1,2] Tetsuya Yamada,[1] Sohei Tsukita,[1,2] Keizo Kaneko,[2] Yuta Shirai,[1,2] Yuichiro Munakata,[1,2] Yasushi Ishigaki,[2] Junta Imai,[2] Kenji Uno,[2] Yutaka Hasegawa,[2] Shojiro Sawada,[2] Yoshitomo Oka,[2] and Hideki Katagiri[1]

[1]*Department of Metabolic Diseases, Center for Metabolic Diseases, Tohoku University Graduate School of Medicine, Sendai, Japan; and* [2]*Division of Molecular Metabolism and Diabetes, Tohoku University Graduate School of Medicine, Sendai, Japan*

Submitted 1 August 2012; accepted in final form 3 December 2012

Takahashi K, Yamada T, Tsukita S, Kaneko K, Shirai Y, Munakata Y, Ishigaki Y, Imai J, Uno K, Hasegawa Y, Sawada S, Oka Y, Katagiri H. Chronic mild stress alters circadian expressions of molecular clock genes in the liver. *Am J Physiol Endocrinol Metab* 304: E301–E309, 2013. First published December 4, 2012; doi:10.1152/ajpendo.00388.2012.—Chronic stress is well known to affect metabolic regulation. However, molecular mechanisms interconnecting stress response systems and metabolic regulations have yet to be elucidated. Various physiological processes, including glucose/lipid metabolism, are regulated by the circadian clock, and core clock gene dysregulation reportedly leads to metabolic disorders. Glucocorticoids, acting as end-effectors of the hypothalamus-pituitary-adrenal (HPA) axis, entrain the circadian rhythms of peripheral organs, including the liver, by phase-shifting core clock gene expressions. Therefore, we examined whether chronic stress affects circadian expressions of core clock genes and metabolism-related genes in the liver using the chronic mild stress (CMS) procedure. In BALB/c mice, CMS elevated and phase-shifted serum corticosterone levels, indicating overactivation of the HPA axis. The rhythmic expressions of core clock genes, e.g., *Clock*, *Npas2*, *Bmal1*, *Per1*, and *Cry1*, were altered in the liver while being completely preserved in the hypothalamic suprachiasmatic nuculeus (SCN), suggesting that the SCN is not involved in alterations in hepatic core clock gene expressions. In addition, circadian patterns of glucose and lipid metabolism-related genes, e.g., *peroxisome proliferator activated receptor* (*Ppar*) α, *Ppar*γ*-1*, *Ppar*γ*-coactivator-1*α, and *phosphoenolepyruvate carboxykinase*, were also disturbed by CMS. In contrast, in C57BL/6 mice, the same CMS procedure altered neither serum corticosterone levels nor rhythmic expressions of hepatic core clock genes and metabolism-related genes. Thus, chronic stress can interfere with the circadian expressions of both core clock genes and metabolism-related genes in the liver possibly involving HPA axis overactivation. This mechanism might contribute to metabolic disorders in stressful modern societies.

stress; liver clock; metabolic disorders; hypothalamus-pituitary-adrenal axis

VARIOUS BEHAVIORAL AND PHYSIOLOGICAL processes, including feeding behavior and energy metabolism, exhibit circadian (i.e., 24-h) rhythmicity, which may play a role in maintaining functional homeostasis. These rhythms are regulated by the circadian clock system, which is composed of transcriptional/translational feedback loops. Although the mammalian master pacemaker is located in the hypothalamic suprachiasmatic nucleus (SCN), the core clock machinery has been identified in almost all peripheral tissues, including the liver (41). In brief, each cell contains a set of core clock genes, such as *Clock*, *Bmal1*, *Cry 1–2*, *Per 1–3*, and nuclear receptors (*Rev-erb*α, *ROR*). The CLOCK/BMAL1 heterodimer regulates the production of proteins such as PERs and CRYs, which in turn regulate the production of BMAL1 (44). Through these feedback loops, the expressions of core clock genes generate endogenous rhythms of numerous protein expressions, leading to rhythmic functioning of cells and tissues over an ~24-h period (12). The molecular clock has been demonstrated to modulate energy metabolism by controlling the expressions and activities of numerous enzymes, transport systems, and nuclear receptors involved in lipid and carbohydrate metabolism (41, 47, 55).

The prevalence of the metabolic syndrome, which represents a spectrum of metabolic and cardiovascular disorders, continues to increase at an alarming rate in modern societies. Responses to an unbalanced diet and lack of physical exercise increase the risk of this pathological condition. In addition, recent evidence suggests that metabolic disorders are associated with the settings of the circadian clock system (6, 26), and moreover that alterations in these settings are among the possible causes of metabolic disorders. For instance, homozygous *Clock* mutant mice become obese and develop metabolic syndrome (50). Disruption of *Rev-erb*α in mice leads to dysregulation of several genes involved in lipid metabolism and alters serum lipid profiles (30). A study using tissue-specific ablation of *Bmal1* demonstrated that clocks in the liver do indeed contribute to glucose homeostasis (29).

Stress is defined as any situation capable of perturbing physiological or psychological homeostasis (38). Health disorders that are associated with dysfunction of the stress system are now major problems in western societies (9). The stress response system consists of the hypothalamus-pituitary-adrenal (HPA) axis and its end-effectors, glucocorticoid receptors. Organisms have developed behavioral and physiological adaptations to the strong influences of day/night cycles, as well as to unforeseen, random stress stimuli. In addition, stress responses and the circadian clock communicate with one another at different signaling levels, resulting in interrelated regulatory networks, and dysregulation of either system can lead to the development of metabolic disorders (10, 35). Indeed, glucocorticoids, which are well known to affect metabolic conditions, entrain the circadian rhythm by phase-shifting the expressions of several core clock genes in peripheral organs, including the liver, kidneys, and heart (5). Therefore, we hypothesized that chronic stress affects the circadian rhythm of core clock gene expressions in the liver via the HPA axis, followed by alterations in metabolism-related genes. The

Address for reprint requests and other correspondence: T. Yamada, Dept. of Metabolic Diseases, Center for Metabolic Diseases, Tohoku Univ. Graduate School of Medicine, 2-1 Seiryo-machi, Aoba-ku, Sendai 980-8575, Japan (e-mail: yamatetsu-tky@umin.ac.jp).

chronic mild stress (CMS) procedure is widely used for analyzing stress effects in experimental animal models (34, 38, 39, 53). To test our hypothesis, we examined the influences of CMS on circadian clock gene expressions in the liver.

MATERIALS AND METHODS

Animals. Eight-week-old male C57BL/6 mice and BALB/c mice (CLEA Japan, Tokyo, Japan) were obtained and maintained under specific pathogen-free conditions. Mice were maintained under controlled temperature and humidity on a 12:12-h light (0900–2100)-dark (2100–0900) cycle. They were housed individually and given a standard laboratory diet (65% carbohydrate, 4% fat, 24% protein) and water ad libitum unless otherwise noted. At 9 wk of age, they were divided into two groups, one continuously housed as stated above (control) and the other subjected to 1 wk of unpredictable CMS. At 10 wk of age, 24 mice of each strain were killed by cervical dislocation at 6-h intervals over 24 h (2, 4, 28, 46) to obtain liver and brain samples at zeitgeber times (ZTs) 3, 9, 15, and 21 in which ZT 0 is defined as lights on and ZT 12 as lights off (n = 6/group for each observation point). All animal studies were conducted in accordance with the institutional guidelines for animal experiments and were approved by Tohoku University.

CMS procedure. The stress protocol was slightly modified from those used in previous reports (34, 38). Briefly, there was one 16-h period of water deprivation; two periods of continuous overnight illumination; two periods (7 and 17 h) of 45° cage tilt; one 17-h period in a cage without bedding chips; one period (8 h) of food deprivation; and one 17-h period of paired housing. All individual stressors used had been classified as "mild" according to the Animals (Scientific Procedures) Act of 1986 (United Kingdom legislation). Animals were left undisturbed in their home cages for 24 h before death.

Measurement of food intake. Food intake was measured during the day after the last day of the CMS procedure, based on division into light (ZT 0 through ZT 12) and dark (ZT 12 through ZT 0) phases.

Blood analysis. Blood glucose levels were assayed with Antsense II (Horiba Industry, Kyoto, Japan) (51). Serum insulin and leptin levels were determined with enzyme-linked immunosorbent assay (ELISA) kits (Morinaga Institute of Biological Science, Yokohama, Japan) (51). Plasma corticosterone levels were assessed using an ELISA kit (ASSAYPRO, St. Charles, MO).

Laser microdissection. All animals were killed by cervical dislocation at the indicated ZTs. The brains were immediately frozen in isopentane on dry ice and stored at −80°C until RNA purification. Coronal cryostat sections (25 μm) through the bilateral SCN of the hypothalamus were placed on PEN-coated slides (Leica Microsystems). Laser microdissections were carried out on a Leica AS LMD (Leica Microsystems) (26). Immediately after microdissection, total RNA was purified, as described below.

RNA purification and quantitative real-time PCR. Total RNA from the liver was purified using an RNeasy minikit (QIAGEN, Valencia, CA) (51). Total RNA from laser microdissected SCN specimens was purified using an RNeasy microkit (QIAGEN) (26). cDNA synthesized from total RNA was evaluated using a real-time PCR quantitative system (Light Cycler Quick System 350S; Roche Diagnostics, Mannheim, Germany) as previously reported (51). Expression levels were normalized against the levels of *β-actin* (for liver) or *gapdh* (for SCN). The sequences of forward and reverse primers were as follows: *Clock*, forward, 5′-AGATCAGTTCAATGTCCTCA-3′; *Clock*, reverse, 5′-TGTCGAATCTCACTAGCATC-3′; *Bmal1*, forward, 5′-ATGAACCCGTGGACCAAG-3′; *Bmal1*, reverse, 5′-CCTGGAATGCCTGGAACA-3′; *Npas2*, forward, 5′-CAGCAGCCACCACCCTATT-3′; *Npas2*, reverse, 5′-TGCGGAGGTGTAGACTGTGT-3′; *Per1*, forward, 5′-GTACTTTGGCAGCATCGACTC-3′; *Per1*, reverse, 5′-CGGTCTTGCTTCAGCACAGA-3′; *Per2*, forward, 5′-CAGCCACCCTGAAAAGGA-3′; *Per2*, reverse, 5′-GTGAGGGACACCACACTCTC-3′; *Cry1*, forward, 5′-CGGTGGAAATTGCTCTCA-3′; *Cry1*, reverse, 5′-GGCATCCTCTTCCTGACTA-3′; *Pparγ-coactivator-1α* (*Pgc-1α*), forward, 5′-ATACCGCAAAGAGCACGAGAAG-3′; *Pgc-1α*, reverse, 5′-CTCAAGAGCAGCGAAAGCGTCACAG-3′; *peroxisome proliferator activated receptor* (*Ppar*) *α*, forward, 5′-TCCCTGTTTGTGGCTGCTAT-3′; *Pparα*, reverse, 5′-TTGGGAAGAGGAAGGTGTCA-3′; *Pparγ*, forward, 5′-TGAGACCAACAGCCTGAC-3′; *Pparγ*, reverse, 5′-GGTTCACCGCTTCTTTCA-3′; *fatty acid synthase* (*Fas*), forward, 5′-TGCTCCCAGCTGCAGGC-3′; *Fas*, reverse, 5′-GCCCGGTAGCTCTGGGTGTA-3′; *sterol regulatory element-binding protein 1c* (*Srebp1c*), forward, 5′-CATGGATTGCACATTTGAAG-3′; *Srebp1c*, reverse, 5′-CCTGTGTCCCCTGTCTCA-3′; *phosphoenolepyruvate carboxykinase* (*Pepck*), forward, 5′-TTGCCTGGATGAAGTTTGAT-3′; *Pepck*, reverse, 5′-GGCATTTGGATTTGTCTTCACT-3′; *glucose-6-phosphatase* (*G6Pase*), forward, 5′-AAAGAGACTGTGGGCATCAATC-3′; *G6Pase*, reverse, 5′-AATGCCTGACAAGACTCCAGCC-3′; *β-actin*, forward, 5′-TTGTAACCAACTGGGACGATATGG-3′; *β-actin*, reverse, 5′-GATCTTGATCTTCATGGTGCTAGG-3′; *Gapdh*, forward, 5′-TGAAGGTCGGTGTGAACG-3′; and *Gapdh*, reverse, 5′-CCATTCTCGGCCTTGACT-3′.

Western blot analysis. Liver extracts were prepared using 20 mmol/l Tris, pH 7.5, 150 mmol/l NaCl, 10% glycerol, 1% Triton X-100, 1 mmol/l ethylendiaminetetraacetic acid, 2 mmol/l Na_3VO_4, 1 mmol/l phenylmethylsulfonyl fluoride, 10 μg/ml aprotinin, and 10 μg/ml leupeptin, and insoluble proteins were removed by centrifugation at 13,500 *g*. Protein content was determined employing a Bradford assay with Bio-Rad Protein Assay reagent (Bio-Rad Laboratories, Hercules, CA). Protein extracts were resolved by SDS-PAGE. Blots were incubated with antibody to PER1 (Santa Cruz Biotechnology, Santa Cruz, CA) and then reincubated with a secondary horseradish-conjugated antibody. Immunoreactive bands were visualized by enhanced chemiluminescence.

Statistical analysis. The results are presented as means ± SE. Two-way ANOVA followed by Bonferroni's post hoc test was used to determine variance with respect to time and mouse group (n = 6 mice/observation point for each group) (2, 21, 26). All experiments were performed at least three times to confirm that the data presented in Figs. 1–7 were reproducible.

RESULTS

CMS alters circadian mRNA expression profiles of core clock genes in the livers of BALB/c mice. First, to examine the influence of chronic stress on circadian clock gene expressions in the liver, BALB/c mice were divided into two groups: one was housed under ordinary conditions (Control-BALB) and the other was subjected to CMS (CMS-BALB) (34, 38, 39, 53). Serum parameters and hepatic gene expressions were analyzed 1 day after the last day of CMS (Fig. 1). In CMS-BALB mice, serum levels of corticosterone, a major glucocorticoid in rodents, were significantly upregulated, and their peak time

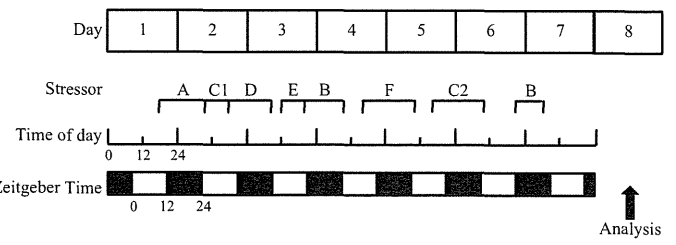

Fig. 1. Schedule of the chronic mild stress (CMS) procedure. Square brackets indicate the time that the stressor was applied to experimental mice. A, one 16-h period of water deprivation; B, two 12-h periods of continuous overnight illumination; C1, one 7-h period of 45° cage tilt; C2, one 17-h period of 45° cage tilt; D, one 17-h period in a cage without bedding chips; E, one 8-h period of food deprivation; F, one 17-h period of paired housing.

points were altered (2-way ANOVA; $F = 8.0731$, $P = 5.0 \times 10^{-4}$) (Fig. 2*A*), indicating activation and altered rhythmicity of the HPA axis in response to this CMS procedure. Body weights and serum leptin levels under CMS conditions were similar to those of the control. Blood glucose levels were also similar, whereas serum insulin levels were higher at one circadian time point in CMS-BALB (2-way ANOVA; $F = 4.2929$, $P = 1.11 \times 10^{-2}$) than in Control-BALB mice (Fig. 2*B*). The food intake amounts were measured on the day after the last day of CMS based on division into light and dark phases, but the CMS procedure did not significantly alter the food intake amount in either phase (Fig. 2*C*). To examine the hypothesis that CMS affects hepatic expressions of core clock genes, we analyzed the circadian expressions of transcripts encoding CLOCK, NPAS2, BMAL1, PER1, PER2, and CRY1 in the livers of both groups. As shown in Fig. 3, the expressions of *Npas2* (2-way ANOVA; $F = 17.0963$, $P < 1.0 \times 10^{-4}$) and *Bmal1* (2-way ANOVA; $F = 15.3862$, $P < 1.0 \times 10^{-4}$) were significantly altered at several circadian time points in CMS-BALB mice. Interestingly, rhythms of *Clock* (2-way ANOVA; $F = 19.3284$, $P < 1.0 \times 10^{-4}$), *Per1* (2-way ANOVA; $F = 30.8876$, $P < 1.0 \times 10^{-4}$), and *Cry1* (2-way ANOVA; $F = 7.4773$, $P = 6.0 \times 10^{-4}$) expressions in the liver were significantly altered in CMS-BALB mice, whereas *Per2* expression levels remained unaltered (Fig. 3*A*).

In addition, immunoblotting revealed the oscillation of PER1 protein expression. The PER1 protein levels oscillated with circadian phases, showing the highest levels at ZT 3 in CMS-BALB mice and at ZT 21 in Control-BALB mice (Fig. 3*B*). These findings are consistent with previous studies showing protein cycles to be delayed by about 6–12 h relative to the mRNA cycles, under both control and stressed conditions (13, 16). Thus, CMS altered the expression rhythms of PER1 on not only the mRNA but also the protein level in the livers of BALB/c mice.

Collectively, these findings suggest that chronic stress alters the profiles of rhythmic core clock gene expressions in the liver and generates gene-specific modulations of circadian expression patterns.

Phase alignments of the core clock genes in peripheral tissues are controlled to be expressed in a synchronized manner by the neurons of the hypothalamic SCN (6). Therefore, we next examined the core clock gene expressions in the SCN of both CMS-BALB and Control-BALB mice. Interestingly, the core clock gene expressions in the SCN showed no significant alterations in either levels or rhythmicity (Fig. 4). Thus, the central master clock is not responsible for alterations in hepatic clock gene expressions under conditions of chronic stress in BALB/c mice.

CMS does not alter circadian mRNA expression profiles of core clock genes in the livers of C57BL/6 mice. A variety of so called "zeitgebers" ("time givers"), such as food and light presence and endogenous glucocorticoid levels, are able to entrain the phase of circadian clocks (23). The CMS procedure used in this study includes water deprivation, food deprivation, and 12-h overnight illumination. In addition, as described above, this CMS procedure altered the endogenous glucocorticoid levels in BALB/c mice (Fig. 2*A*). On the other hand, C57BL/6 mice do not display activation of the HPA axis when exposed to chronic stress (24, 43). Furthermore, the same CMS procedure was confirmed to have no effect on serum cortico-

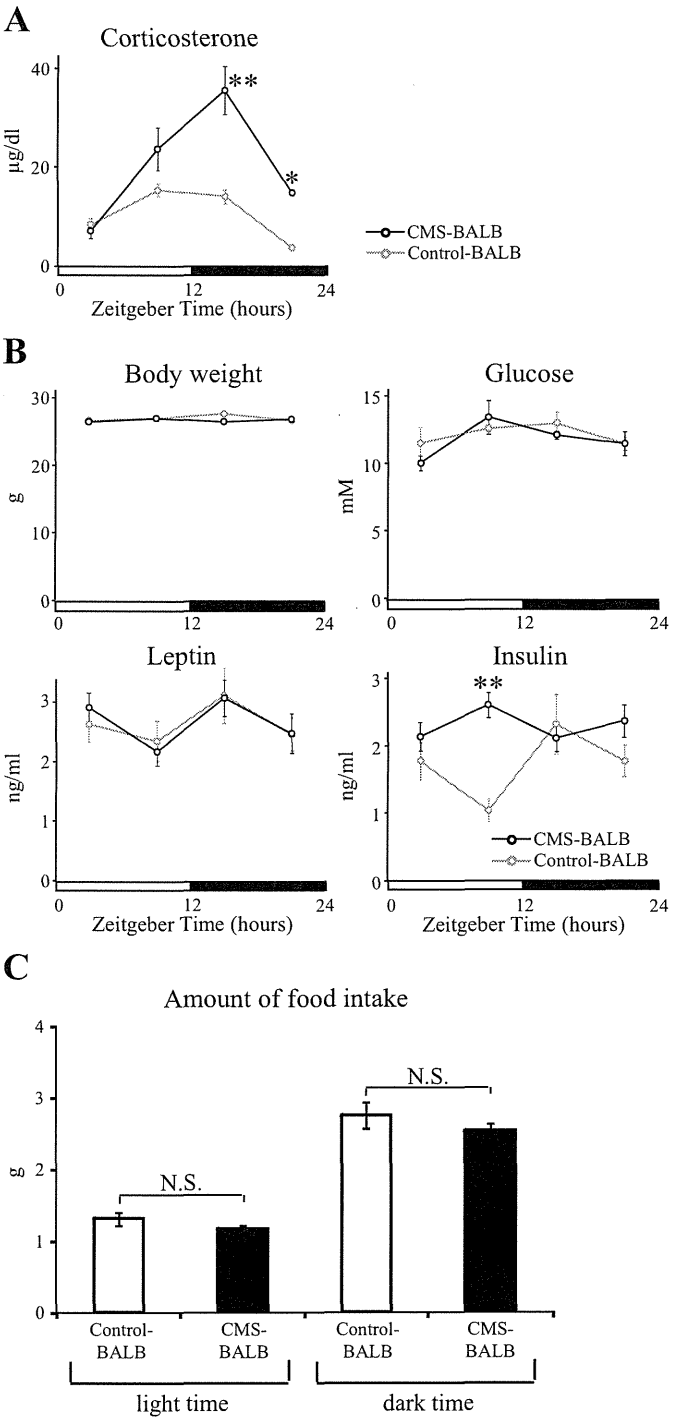

Fig. 2. Metabolic parameters of BALB/c mice. Mice were assigned to either the Control-BALB or the CMS-BALB group. Diurnal variations in plasma corticosterone (*A*), body weight, blood glucose, plasma insulin, and leptin (*B*) are shown; $n = 6$ mice/group for each observation point. Results are expressed as means ± SE. Two-way ANOVA was used to determine variance with respect to time and groups, followed by Bonferroni's post hoc test ($^*P < 0.05$ and $^{**}P < 0.01$). *C*: food intake was measured 1 day after the last day of the CMS procedure, with division into light and dark phases. Results are expressed as means ± SE. One-way ANOVA was used to determine statistical significance (N.S., not significant).